DEVELOPING A SCAFFOLD FROM

PORCINE ADIPOSE TISSUE

By

KEVIN D. ROEHM

Bachelor of Science in Biosystems Engineering

Oklahoma State University

Stillwater, OK

2013

Submitted to the Faculty of the
Graduate College of the
Oklahoma State University
in partial fulfillment of
the requirements for
the Degree of
MASTER OF SCIENCE
December, 2014

DEVELOPING A SCAFFOLD FROM

PORCINE ADIPOSE TISSUE

Thesis Approved:

Dr. Sundar Madihally

Thesis Adviser

Dr. Danielle Bellmer

Dr. Joshua Ramsey

ACKNOWLEDGEMENTS

My sincere thanks go to Dr. Sundar Madihally, my advisor, who fostered my interest in tissue engineering and inspired me to continue research. Without him this thesis would never have been written. I also wish to acknowledge Jessica Hornberger who first imagined porcine adipose tissue as a scaffold and contributed to the early stages of this project before she was forced to abandon it. I would like to thank my committee members, Dr. Danielle Bellmer and Dr. Josh Ramsey, for their assistance with this project and their feedback on it.

Moreover, I would like to thank my colleagues Jimmy Walker, Christian Tormos, and Kumar Singarapu for assisting me with cell culture and Nicholas Flynn, Jorge Lightfoot, and Dr. Babu Fathepure for assisting me with DNA extraction, gel electrophoresis, and imaging.

Name: KEVIN D. ROEHM

Date of Degree: DECEMBER, 2014

Title of Study: DEVELOPING A SCAFFOLD FROM PORCINE ADIPOSE TISSUE

Major Field: CHEMICAL ENGINEERING

Abstract: Tissue engineering aims to address the critical lack of immunocompatible tissues and organs available for grafting and transplantation. Scaffolds are three dimensional, porous structures that provide shape and attachment sites for cells during tissue growth and are a critical component of tissue engineering. Naturally derived scaffolds have seen significantly greater clinical usage than synthetic scaffolds and have marked advantages, including naturally present growth factors and ideal morphology. In addition, scaffolds derived from xenogeneic tissues are advantageous because human tissues are difficult and costly to obtain. However, careful decellularization is required to prevent immune rejection. Porcine adipose tissue (PAT) is inexpensive and readily obtained. This study's objective was to develop a general tissue scaffold from PAT while maintaining the structure of its extracellular matrix (ECM). Maintaining PAT's ECM intact is expected to improve nutrient distribution and cell ingrowth. Two decellularization methods were attempted: methanol-chloroform submersion, and freeze-thawing. Methanol-chloroform submersion destroyed the tissue and was discontinued; freeze-thawing was successful and pursued: the number of freeze-thaw steps (1 – 7), the tissue surface area and thickness, and the trypsin incubation time (1 – 3 hours) were evaluated and optimized. Moreover, following an initial cell seeding study during which cell attachment and ingrowth did not occur, a lipid removal strategy using sonication (20 – 60 minutes with water, trypsin, or SDS) and immersion in xylene (20 seconds to 20 minutes) was also devised to remove all lipids and thereby create a hydrophilic environment conducive to cell seeding. Processed scaffold mechanical strength and morphology were examined using histology slides and SEM digital micrographs. An additional cell seeding study using CFDA-SE stained cells was conducted. An average ultimate tensile strength of 87.4 kPa, an average break strain of 53.9 kPa, an average elastic modulus of 324 kPa, 30% relaxation per ramp, and intact morphology, including tubular vascular channels were found. Cells examined in micrographs of seeded tissue demonstrated successful cell ingrowth and uniform distribution at 8 days. Overall, an optimized decellularization process and a lipid removal processes were developed that retained natural tissue morphology. Moreover, obtained scaffolds compared favorably with small intestine submucosa (SIS), a clinically available scaffold.

TABLE OF CONTENTS

LIST OF TABLES

LIST OF FIGURES

CHAPTER I

INTRODUCTION

1.1 NEED FOR TISSUE ENGINEERING

Organ transplantation and tissue grafting are both prevalent medical procedures. However, they face traditionally insurmountable drawbacks. First, organs are not perfectly matched to patients and immunosuppressant therapies are required to prevent transplant rejection [1]. Second, disease transmission is a significant risk [2]. Third, organ transplant waiting lists are extensive. To illustrate, in 2012 there were approximately 58 thousand patients on the kidney transplant wait list. However, only about 18 thousand transplants were performed that year. In addition to this three-fold disparity between transplants and wait-listed patients, between 2011 and 2012 the number of candidates awaiting a transplant increased by 3% while the number of transplants performed decreased by 1.7% [3]. This situation is untenable and an alternative is desperately needed.

Concerning tissue grafts, they are widely used for repair and reconstruction. Blood vessels are excised and implanted during bypass surgeries, nerves are excised for motor neuron reconstruction and skin is excised for facial reconstruction and burn treatment. These autografts, tissue grafts coming from other parts of the patient's body, represent the "gold standard" or most desired material because 1) the risk of rejection is eliminated and 2) the tissue is immediately available without any transport logistics or wait-lists for genetically similar tissue to become

available. However, autografts require a secondary operating site, increasing the risk of infection by placing additional load on the patient's immune system and forcing the body to heal additional damage. In addition, donor site morbidity, comprised of a variety of complications arising from removal of tissue, is another issue with the use of autografts [4-6]. Allografts represent the main alternative to autografts. Tissue transplanted within the same species between different individuals, allografts face the same challenges as donor organs; a lack of supply, a risk of rejection, and the possibility for disease transmission from the donor.

Tissue engineering seeks to replace grafts and donor organs alike using *in vitro* engineered tissues. By engineering tissues, patients' own cellular material can be used, significantly reducing or eliminating the risk of rejection while substantially increasing the availability of transplants and grafts. In addition, obtaining cells is much less invasive than excising tissue and only a relatively small number of cells are required.

A typical tissue engineering cycle is shown in Figure 1.1. First, cells are obtained from the patient. A variety of stem cell and progenitor cell sources are possible. Second, cells are cultured with growth medium until a sufficient number of cells is present. Third, cells are seeded onto a scaffold. Fourth, the seeded scaffold is placed in a bioreactor which supplies a continuous stream of nutrients (typically growth medium) while carrying away cell waste as the cells spread through and establish themselves in the scaffold. A bioreactor may be as simple as a tissue culture dish with regularly changed growth medium or as complex as a system that pumps media through the scaffold, inducing a desired stress on the scaffold to assist cell growth. Fifth, the seeded scaffold is implanted into the patient. It is worth noting that many scaffolds are implanted directly, bypassing the cycle shown in Figure 1.1. Instead of *in vitro* cell seeding and cell growth in a bioreactor, the *in vivo* environment of the body supplies cells and nutrients to the graft. This approach eliminates seeding and growth time required before implantation. However, direct implantation is impossible when immediate tissue functionality is required.

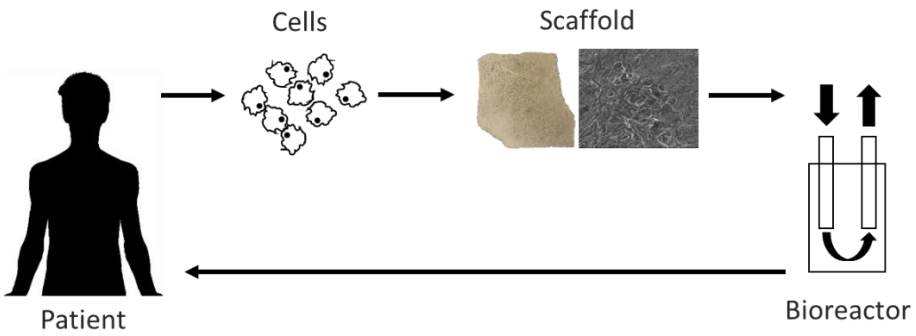

Figure 1.1: A typical tissue engineering cycle

1.2 HYPOTHESIS AND OBJECTIVES

Naturally derived matrixes from various tissues such as small intestine, bladder, and skin have been used to support and guide the in-growth of cells and have shown promise in clinical applications [7]. To avoid an immune reaction due to mismatch, cells and DNA components are carefully removed without altering the source tissue's extracellular matrix (ECM) distribution. However, these tissue matrixes are limited by source and large-scale preparations. This is attributed to the heterogeneity in biophysical properties such as permeability, thickness, and matrix composition which affect the quality and reliability of the regenerated tissue in clinical practice. While a variety of specific like-to-like scaffolds (where decellularized human cadaverous tissue is used to replace the same tissue in a patient) have seen clinical usage [8], there is a need for general scaffolds which can be used to replace a variety of different tissues. The objective of the work represented in this thesis is to develop a general soft tissue scaffold from a readily available, inexpensive source, while maintaining the tissue's native morphology. Maintaining the morphology intact is expected to improve cell viability, nutrient distribution, and cell ingrowth.

According to the U.S. Department of Agriculture's (USDA's) National Agricultural Statistics Service (NASS) [9], in 2013, 5.42 million pigs were slaughtered in Oklahoma. Moreover, porcine adipose tissue obtained from the dorsal ridge of swine, colloquially known as pig back-fat or fatback, is relatively inexpensive and is often discarded during processing. A local supplier priced

pig back fat at $1.05 per pound (personal communication, October 17, 2014). In addition, small intestine submucosa (SIS), such as scaffolds produced by Cook Biotech, is obtained from carefully controlled, pathogen free pigs in processes approved by The United States Food and Drug Administration (US FDA). Therefore, porcine adipose tissue (PAT), specifically pig back fat, was chosen as the source for this study. To meet the objective, two specific aims were formulated:

1. *Create a process that decellularizes PAT while maintaining its natural morphology*.

   Two decellularization methods were examined. The first method used a 1:1 mixture of methanol and chloroform. This method destroyed PAT's ECM and was discontinued. A second method, freeze-thawing, was chosen for examination based upon its use in literature to decellularize PAT. Freezing and thawing the tissue repeatedly did not damage the tissue's morphology. Therefore, the decellularization portion of the second method was optimized. Further, the success of each optimization point was evaluated through light microscopy of Hematoxylin and Eosin (H&E) stained slides. A lack of visible cell nuclei indicated successful decellularization. Due to the necessity of lipid removal to match phobicity between the scaffold and growth medium cells are suspended in, a process was developed which removed the lipids from the tissue. The concentration of DNA remaining in the processed scaffold was evaluated through a combination of nanodrop spectrophotometry and gel electrophoresis. Negligible levels of DNA remained in processed PAT. Finally, processed PAT was seeded with cells tagged with a florescent marker. Cells spread throughout the matrix in three-dimensions with even distribution. These analyses demonstrated that the process created a viable tissue scaffold.

2. *Characterize PAT's mechanical and physical properties.*

   To understand the suitability of the scaffold, mechanical testing was conducted and processed PAT was examined via scanning electron microscopy (SEM). First, a traditional tensile test was performed and the ultimate tensile stress and break strain for the scaffold

were determined. Based upon the data obtained through tensile testing, it was confirmed that processed PAT is viscoelastic and multiple-step stress-relaxation (MSSR) testing was conducted. It was determined that processed PAT has mechanical characteristics similar to other soft tissue scaffolds, with predominant comparison to small intestine submucosa (SIS), the most successful commercial scaffold on the market. Through SEM micrographs, processed PAT's porosity and vasculature was examined. Pores in the 150 μm range were examined as were intact vascular tubes.

CHAPTER II

BACKGROUND: SCAFFOLDS FOR TISSUE ENGINEERING

2.1 SCAFFOLDS

Scaffolds are a critical component of the tissue engineering process. They are porous, sponge-like materials that provide the structure of the engineered tissue. The biophysical properties of the scaffold, including its biocompatibility, biodegradability, mechanical properties, and physical structure (porosity, average pore size, pore distribution, etc.) determine its usefulness. Biocompatibility, typically demonstrated through *in vivo* animal models and cell seeding, demonstrates that a scaffold allows cells to grow and will not result in rejection. Cytotoxicity, when a scaffold is toxic to cells, can be examined through cell seeding and must be avoided. However, systemic incompatibility can lead to swelling, immune rejection, or other undesirable host complications and requires an *in vivo* model for evaluation. Biodegradability, particularly controlled biodegradability ensures that the scaffold breaks down as cells grow and begin producing extra cellular matrix (ECM) proteins. The rate of degradation must be such that it allows seeded cells to establish their own ECM network while not hindering the formation of the native ECM network. This concept is especially important when dealing with scaffolds made from synthetic materials, typically polymers that do not co-opt the ECM provided. Naturally derived matrixes comprised of ECM contain the same components as native ECM, matrix turnover, the time required for the scaffold ECM to be replaced by the host's ECM generated by cells after ingrowth may be

determined to provide more relevant insight than degradation in these cases. Scaffold mechanical properties directly affect cellular biochemistry through cell mechanoreceptors [10]. Moreover, mechanical properties direct mesenchymal stem cell (MSC) differentiation towards different cell lineages (neural, myogenic, or osteogenic) [11].

There are two general categories of scaffolds under investigation in literature; they are categorized by material type. First, scaffolds comprised of synthetic materials (polymers and ceramics). Second, scaffolds comprised of ECM components (often derived from native tissues). Overlap between these categories does occur. Some scaffolds are a combination of natural and synthetic materials. In addition, natural polymers, ground ECM, and collagen (a naturally occurring ECM protein) are often processed as if they were synthetic materials. Target tissue dictates materials investigated: ceramics have material properties similar to those of bone and have therefore seen extensive usage as bone scaffolds. Synthetic and natural polymers (such as gelatin, chitosan, and ECM proteins) are popular soft tissue scaffolds because they are not rigid and have characteristics comparable to soft tissues. This thesis is focused on the development of a scaffold for general soft tissue applications and so the focus of this background will only cover soft tissues and the materials used for soft tissue engineering.

2.1.1 Synthetic Scaffolds

A wide range of synthetic polymers are available and are investigated as tissue scaffolds. Poly(lactic-co-glycolic acid) (PLGA) and polycaprolactrone (PCL) are two common synthetic materials under investigation. Numerous techniques are used in the formation of scaffolds from synthetic materials and are separated into two categories: additive and subtractive.

2.1.1.1 Additive Methods

Electrospinning: Electrospinning uses a high voltage current to induce a thread of solvated polymer, extruded from the tip of a nozzle (typically extruded from a syringe using a syringe pump),

to pass through open air to a grounded collector plate. Near total solvent evaporation occurs as the polymer travels between the nozzle tip and the collector plate which can be spun to induce a non-random fiber orientation. Fiber sizes between 50 nm and 30 μm can be obtained using this method [12]. However, unevaporated solvents are a potential drawback of electrospun scaffolds as chloroform and other cytotoxic solvents are used [2]. See [13] for a current review on electrospinning.

3D Printing: Referred to by a variety of names, including solid freeform fabrication and rapid prototyping (RP), RP systems are unique in that they use computer aided manufacturing (CAM) and three dimensional (3D) computer aided design (CAD) models. The CAD model can be almost any 3D structure imaginable. The CAM system creates a path scheme from the CAD model that is executed to build the material layer by layer. Actual printing may be achieved through a nozzle, by using a laser to cross-link a photoreactive polymer or hydrogel, or by fusing a powder. The main limitation of RP is the achievable resolution. For further information refer to [14].

Others: Other additive methods, including layer by layer (LBL) deposition exist [15], although LBL deposition is typically used to create a film with desirable properties on another structure (e.g. an electrospun scaffold).

2.1.1.2 Common Subtractive Methods

Particulate leaching: Particulate leaching is done by mixing a solid particulate, such as salt, with a solvated polymer. After casting the polymer, it is submerged in one of the solid particle's solvents (e.g. water for the salt example). The particulate then leaches out of the scaffold, leaving pores that correspond in size to the original particle distribution.

Gas Foaming: Gas at high pressure is injected into a polymer that creates a semi-connected network of pores of varying size [16].

Freeze Drying: Unlike particle leaching, freeze drying doesn't require a solid particulate. Freezing a solution of polymer dissolved in glacial acetic acid or benzene creates ice crystals which act as the particulate. Lyophilizing (or freeze-drying) the structure extracts the liquid from the scaffold leaving behind a porous structure. The pore size is controlled by the rate of freezing with a greater temperature gradient resulting in smaller pore size and a smaller temperature gradient resulting in larger ice crystals and thereby larger pores [16]. Freeze-dried scaffolds are used in the following, which include multiple natural polymers: [17-19].

2.1.2 Naturally-derived Scaffolds

There are several types of naturally-derived scaffolds. Some of the same production techniques used for synthetic scaffolds are used with natural materials (see freeze-drying references above). Decellularized tissues can be ground into powders and then formed into the desired shape by compression or by other means. However, maintaining native tissue morphology during the decellularization process has two key advantages: 1) a natural porous structure created by voids previously inhabited by cells eliminate the need for additional processing to obtain a porous architecture and 2) intact vasculature from blood vessels and capillaries are expected to improve nutrient flow throughout the scaffold. However, depending on the tissue in question, removing the cellular material without damaging the structure of the scaffold can represent a significant challenge.

A wide variety of decellularization methods have been presented in the literature. Perfusion, pumping detergent through whole organ or tissue vasculature is common, especially in whole organs (refer to [20] for an example of perfusion). Tissues may be immersed in detergents with or without agitation or other mechanical assistance, cyclically frozen and thawed, and/or enzymatically digested. Numerous methods used in literature are listed by Gilbert et al. [21] and Crapo et al. [22] along with their mode of action and effects on the ECM. Table 2.1 provides a series of decellularization methods that have been applied to adipose tissue.

Table 2.1: Decellularization methods applied to PAT with references

Method	Reference
Mechanical:	
Freeze/thaw	[23-26]
Homogenization	[5]
Freeze-drying	[24, 25, 27]
Massaging	[27]
Detergents:	
Sodium deoxycholate	[23, 27]
Sodium dodecyl sulfate (SDS)	[27, 28]
Triton X-100	[23, 24, 27]
Solvents:	
Isopropanol	[24-26]
Enzymatic:	
DNase	[23, 24]
RNase	[28]
Trypsin	[24-27]

2.1.3 Comparison between naturally-derived and synthetic scaffolds

Synthetic scaffolds have significant advantages compared to naturally-derived scaffolds. The pore size, mechanical properties, and structure of synthetic scaffolds are generally controllable and these properties are fixed or difficult to control for naturally-derived scaffolds. Rapid prototyping or 3D printing in particular is envisioned as the ideal method that combines printing with 3D imaging to create scaffolds with shape and mechanical properties tailored to each patient [29]. However, synthetic matrixes have failed to show efficacy in clinical applications. ECM contains inherent growth factors that stimulate the growth of the ECM, such as vascular endothelial growth factor (VEGF), transforming growth factor beta (TGF-β), basic fibroblast growth factor (bFGF), placenta growth factor, and insulin-like growth factor 1. These growth factors stimulate ECM protein production [30], encourage angiogenesis, and regulate cell adhesion [31]. These growth factors are not present in synthetic matrixes. An overall comparison between naturally-derived and synthetic scaffolds is shown in Table 2.2.

Table 2.2: Comparison between naturally-derived and synthetic scaffolds

Naturally-derived Scaffolds	Synthetic Scaffolds
Maintains growth factors and other proteins present in native tissues that assist cell seeding	Growth factors may be chemically attached to the scaffold?
Exact organ shape can be obtained by decellularizing whole cadaver organs	Scaffolds can be printed from 3D CAD models
Human tissues are difficult to obtain and in short supply; whole human organs are even more so.	3D printing resolution insufficient
Xenogenic (non-human) tissues can cause inflammation and rejection, decellularization is critical and scaffolds must be tested for remaining DNA content.	Abundant supply of polymers. Require careful screening for biocompatibility and degradation.
Scaffolds from natural sources have been approved by the FDA and are used clinically	Synthetic scaffolds are widely investigated by the scientific community but not used clinically
Natural vasculature can be retained after processing.	—

2.1.4 Drawbacks of Available Naturally-Derived Scaffolds

Two of the best known, clinically available scaffolds are SIS and acellular dermis (or skin). A review by Badylak [32] lists several clinically available products from porcine SIS, human and bovine dermis, bovine and horse pericardium, and human fascia lata. Porcine SIS and human, porcine, or bovine dermis represented the majority of the scaffolds available. Despite the clinical success of SIS, these scaffolds all have key disadvantages. First, the anatomical source of the unprocessed material drastically affects the properties and quality of the obtained scaffold, even within a relatively small area (for this effect in SIS see [33]). Second, only greatly limited thicknesses can be obtained. SIS ranges in thickness from approximately 161-247 µm under hydrated conditions [33]. Graftjacket®, a commercially available acellular dermal product, has an upper limit thickness of 1.5 mm. In contrast, dorsal porcine adipose tissue thickness can be up to 16 mm [34].

2.2 DNA Requirements

Native tissues must be decellularized before they can be used as tissue scaffolds. The goal of decellularization is to remove the cellular material, particularly DNA content, which has been shown to be a significant factor in immune rejection. Crapo et al. [22] published guidelines regarding the mass fraction and type of DNA remaining in a scaffold after processing that is sufficient to limit the risk of immune rejection:

- 50 ng double stranded DNA per mg ECM dry weight or less
- DNA fragments less than 200 base pairs
- H&E staining reveals a nuclei-free structure.

Zheng et al. [35] explain the consequences of poor decellularization in a 2004 study on Restore™ SIS, manufactured by Depuy Johnson and Johnson. The group found visible cell nuclei in histology slides of the scaffold and used nested polymerase chain reaction (PCR) to demonstrate DNA was present in the scaffold. Their results demonstrated that allowing the defect to heal without Restore™ implantation resulted in a better outcome than implanting the v scaffold. These results demonstrate the necessity of ensuring DNA removal from the scaffold. DNA evaluation is routinely conducted through methods that are less arduous than PCR. Spectrophotometry using a florescent dye such as PicoGreen or by gel-electrophoresis using dyes such as SYBR-Green or ethidium bromide and Nanodrop spectrophotometry are simple tests that have been used [36]. However, caution must be used when evaluating DNA content through nanodrop spectrophotometry: common organic solvents used in DNA extraction (phenol and chloroform) strongly effect the results of the test and skew the results. Thermo scientific, the manufacture of the nanodrop line of spectrophotometers, suggests that the downstream outcome is the true indicator of DNA quality. In addition to solvent contamination, contamination by proteins can also occur [37]. Therefore, using nanodrop spectrophotometry to measure DNA content without secondary confirmation must be suspect.

2.3 MECHANICAL PROPERTIES

2.3.1 Tissues' Unique Mechanical Properties

Tissue engineering mechanical property characterization is both important and challenging. As stated, scaffolds need to have mechanical properties that mimic those of the native tissue targeted for replacement (section 2.1, first paragraph). Most tissues are anisotropic (they have orientation-dependent mechanical properties). This property in soft tissues is attributed to fiber orientation within the ECM [38]. In addition, all tissues are viscoelastic [39]. Viscoelasticity describes materials that are both elastic and viscous: they store some portion of the deformational energy exerted on them and dissipate the rest of it (elastic materials store all deformational energy and return to their initial state immediately upon relaxation, plastic materials dissipate all deformational energy and do not return to their original state even after force has been removed for an extended period of time). Because of the energy dissipation experienced by viscoelastic materials, they have history-dependent characteristics (i.e. past stresses effect the current stress response of the material).

The complex mechanical behavior of soft tissues is due mainly to collagen. However, in the unstretched state, collagen fibrils are wavy and do not contribute to the mechanical strength of the tissue (the toe region). In the initial portion of this region, elastin. As the tissue is strained, the collagen fibrils straighten (analogous to a spring). As they uncoil, they increasingly contribute to the tissue's stress response until they are fully straightened resulting in the nonlinear stress curvature in the toe region. Once uncoiled, the stress-strain curve becomes approximately linear and collagen dominates (loading region). The result is the non-linear J-shaped stress curve or J-curve typical of soft tissues (the loading portion of Figure 2.1) [40]. In its entirety, Figure 2.1 demonstrates a typical stress-relaxation curve and a typical elastic response, shown for comparison. After the specimen experiences a constant strain-rate stress increase until it reaches a specified extension or strain (the J-curve), the extension (and therefore strain) is held constant and the tissue

is allowed to relax by some overall percent to an asymptotic minimum stress. Conversely, the elastic response is characterized by constant stress at constant strain. This illustrates the difference between elastic and viscoelastic tissues as the viscoelastic tissue dissipates stress and thereby loses energy while a perfectly elastic material has no losses and therefore maintains constant stress.

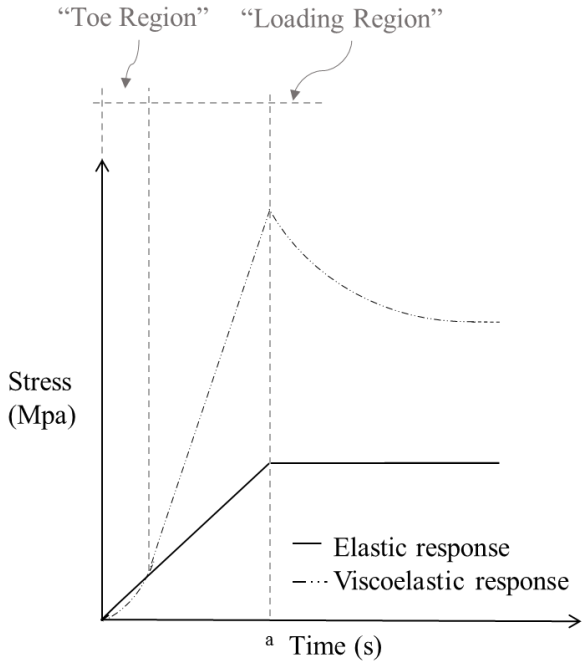

Figure 2.1: Typical elastic and viscoelastic stress response over time. Modified from [41]

2.3.2 Characterizing Tissue Mechanical Properties

2.3.2.1 Describing Mechanical Properties

There is a distinct lack of consistent methods used to describe the mechanical properties of scaffolds based on a diverse set of characterization tools. Hooke's Law, which uses the Young's Modulus (also modulus of elasticity) to model the linear portion of many elastic materials (e.g. steel) cannot properly describe viscoelastic properties except for in very limited regions of strain (some have described tissue properties with an initial and final modulus where the initial modulus roughly approximates the initial portion of the toe region and the final modulus approximates the semi-linear load region [42]). However, the viscoelasticity of tissues is well understood and

constituent models have been developed to describe these properties. One of the most prevalent models is Fung's Quasi-linear-viscoelastic (QLV) model, first described in [43], and still present in recent publications [44-47]. Other models in use include an 8-chain model adapted from the rubber industry [47], the standard linear solid (SLS) model [48], the Helmholtz free energy density function model [49], models using finite element analysis [50], and multiple unique constitutive models created by researchers to describe their particular scaffold or tissue (see [18] for one example). All constitutive models are approximations that aim to characterize the viscoelastic properties of the specified tissue. However, they provide a method of approximating the total mechanical properties of the tissue and may give insight into an approximate mechanistic approximation of the tissue. Additionally, among similarly specified models, like the QLV model with similarly specified elastic responses, parameters may be directly compared [51]. However, unless the model parameters have a mechanistic interpretation, this comparison may be of limited utility when comparing scaffolds for a specific use.

2.3.2.2 Testing Methods

Mechanical testing must be performed before any descriptors of mechanical properties can be obtained. Numerous test protocols and test hardware have been used. Rheology [52, 53], dynamic mechanical analysis (DMA) [54], stress-relaxation [44, 47], multi-step stress-relaxation [18, 46], cyclical testing [18, 45, 47], and creep testing [45] are examples of tests performed to characterize viscoelastic scaffold properties. Each method has advantages and disadvantages. For example, DMA can be used to measure uniaxial sinusoidal properties of tissue while rheology describes sinusoidal shear properties. MSSR can demonstrate history-dependent characteristics, such as whether a scaffold is strain-hardening or strain-softening that the other methods cannot. However, the first stage is typically low strain and may not provide the same quality of data as a single stress-relaxation curve using the full stress range available (load cells exhibit significant noise at low stress). Overall, the relevance and usefulness of a particular test depends upon the

properties of the scaffold, the expected application stresses, and the mechanical property or properties of interest.

Although traditional elastic test methods cannot be used to completely characterize tissue scaffolds, they provide useful information, mainly the ultimate tensile strength and break strain of the scaffold. Both uniaxial tensile and uniaxial compressive testing, the two traditional mechanical testing methods, are widely used to characterize tissues. However, these methods have been modified and additional considerations are required for tissues and scaffolds. For tensile testing, blood vessel and other tubular scaffolds are often tested by placing a short length of tubing over two hooks and straining the material circumferentially (Figure 2.2.a, [55]). For other materials, clamping proves too difficult or impractical and the ends of a sample may be glued directly to the testing apparatus (Figure 2.2.b, [42]) or they may be embedded in blocks of epoxy (Figure 2.2.c, [56]). Embedding must be done with care lest the resin infiltrate the tissue and change its mechanical properties. Concerning, compressive testing, both confined and unconfined testing can be performed. With any hydrated tissue, especially a hydrated tissue not being tested in hydrated conditions, it is important to consider liquid compressibility: unconfined compression allows water to freely escape the scaffold while confined compression prevents liquid from escaping. Therefore, direct comparisons cannot be made between data from unconfined compression testing and data from confined compression testing.

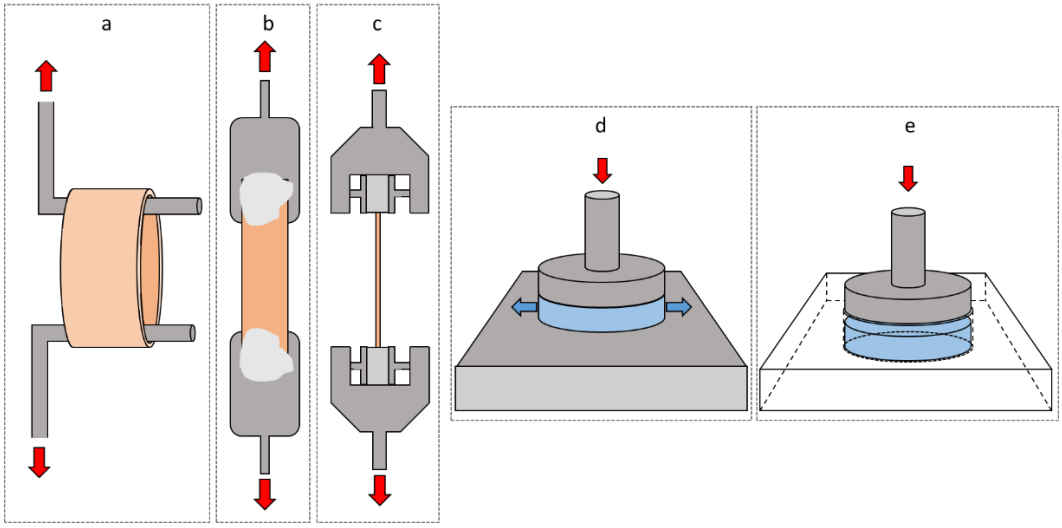

Figure 2.2: Tensile and compressive methods used in tissue engineering. The depicted tensile methods are: a) circumferential testing, b) supergluing the ends of sample to paddles or clamps, and c) embedding tissue ends in epoxy resin. Compressive methods shown depict d) unconfined compression and e) confined compression

2.3.2.3 Hydration and Temperature

Hydration and temperature both play an important role in scaffold mechanical testing. Hatami-Marbini [44] conducted experiments exploring the relation between hydration and elastic modulus. He attributed the hydration dependence of the elastic modulus to proteoglycan's negative charge density; as the matrix is hydrated and swells, the charge density decreases. He pointed to osmotic pressure change as an additional contributing factor. Hydration is not an important factor for certain polymers, such as PCL. However, temperature is still an important consideration [47]. Overall, it is best practice to conduct all testing in a physiological solution such as phosphate buffered saline (PBS) at 37°C to match tonicity, hydration, and temperature of expected implant conditions.

2.3.2.4 Anisotropic Considerations

Many tissues have anisotropic properties. Bone, tendon, and muscle are well-known anisotropic materials. In soft tissues, like tendon, the anisotropy is attributed to fiber orientation within the ECM of the tissue. Many researchers mimic mechanical anisotropy using electrospinning with aligned fiber orientation. Şenel Ayaz et al. [38] demonstrate one method to form an anisotropic scaffold via electrospinning and demonstrate that the anisotropy is due to fiber alignment in the scaffold.

In addition to recognizing and creating anisotropic materials, multiple methods have been described to conduct multi-dimensional mechanical testing. These include using a sphere of known weight to indent the surface of the material [57], using a set of hooks attached around the periphery of a sample with two movable arms (x and y) and a CCD camera to record strain [39], and atomic force microscopy (AFM) [58]. As with viscoelastic testing, the relevance of any test is related to the physiological stresses applied to the tissue or scaffold and the properties of interest. For example, lung tissue does not experience uniaxial tensile or uniaxial compressive stress. Instead the material of the lung experiences a multi-axial stress as the lungs expand and contract.

2.3.3 Aside: Elasticity vs. stiffness

On a side note, when discussing mechanical properties, there is some confusion concerning stiffness and elasticity. Stiffness is a property of a specific, dimensionally defined object. Elastic modulus has no dimensional dependency; it is purely an intrinsic material property. Moreover, the engineering definition of stiffness is the force required to cause a material to deflect by a given distance ($k = \frac{F}{\delta}$, where k is the stiffness, F is the applied force, and δ is the resulting linear deformation). The elastic modulus is the ratio between the stress a material experiences and the corresponding strain it experiences. It is a measure related to stiffness of a sample, but it is not directly stiffness. To illustrate, stiffness may be calculated using the elastic modulus and

dimensional parameters. For axial loading, stiffness can be calculated as follows: $k = \frac{AE}{L}$, where k is the stiffness (or spring constant) in units of, A is the cross-sectional area, E is the elastic modulus, and L is the length of the element (along the line of load) [59].

CHAPTER III

MATERIALS AND METHODS: OBTAINING AND ANALYZING PROCESSED PAT

Porcine adipose tissue was obtained from Ralph's Meat Packing Company, Perkins, OK.

3.1 METHOD 1

Samples weighing approximately 150 mg were cut by hand. They were immersed in 100% ethanol for 45 minutes and placed in a 1:1 methanol and chloroform mixture for 30, 60, 90, and 120 minutes. Samples were rinsed with PBS and incubated in trypsin-EDTA, a proteolytic enzyme, (0.05% GIBCO, Life Technologies, Grand Island, NY.), at 36°C for 1 hour. They were rinsed with PBS again and placed in micro-centrifuge tubes. A solution of 0.5% (wt/v) SDS (> 95%, Sigma Aldrich, St. Louis, MO) in 0.9% saline was added and the samples were vortexed for 15 or 30 minutes. Then samples were homogenized, an additional 200µL SDS was added. The samples were centrifuged, and visually examined.

3.2 METHOD 2

PAT samples were sectioned by one of two methods. First, samples were cut by hand using a razorblade to approximately 1cm×1cm×1-2mm or 3cm×3cm×~2mm. Second, samples were cut using a meat slicer to approximately 3cm×3cm and either 1 or 2 mm thick. The final process, shown in Figure 3.1, works with larger samples sectioned using a meat slicer. The decellularization portion of the process (all steps leading up to sonication) was optimized by selecting a relevant

range of values and preparing samples at intervals over the range (Table 3.1). Outcomes were evaluated through routine light microscopy of histology slides stained with H&E.

Table 3.1: Decellularization Optimization

Method	Ethanol Concentration	Freeze Temp (ºC)	Number of Cycles	Thaw Time (min)	Trypsination time at 37ºC (hr)	Approximate Sample Size
1	30%					
2	50%	-81	1	20	1.0	~ 1x1x.2 cm
3	70%					
4			1			
5	50%	-81	2	20	1.0	~ 1x1x.2 cm
6			3			
7			4			
8					1.0	
9	50%	-81	4	20	1.5	~ 1x1x.2 cm
10					3.5	

The remaining process was developed to remove lipids from the tissue. In detail, the steps are as follows:

i) The ethanol fraction (in DI water) of the freezing solution was varied between 30%, 50%, 70%, 80%, and 90% ethanol.

ii) The number of freeze-thaw cycles was varied from 1 to 7. For all of the freeze-thaw cycles, samples were placed in a -80°C freezer for a minimum of 1 hr and were examined upon removal for freezing. In the presence of unfrozen solution, the samples were placed back into the freezer until freezing was successful. This temperature was sufficient to freeze ethanol solutions below 80%. Thawing was conducted for either 20 minutes or 1 hour at either ambient temperature or 37 °C. Moreover, samples were either frozen from initial ambient temperature or from an initial temperature of 1 °C.

iii) Upon completion of the last freeze-thaw cycle, samples were rinsed with PBS and incubated in trypsin-EDTA (0.05% GIBCO) at 37ºC for 1, 1.5, and 3.0 hours.

iv) Samples were rinsed with deionized water and sonication was performed in a water bath sonicator (Fisher Scientific FS20 Sonic Cleaner) either for 20 minutes or 1 hour. During sonication, samples were immersed in a beaker containing 0.5% (wt/v) SDS in 0.9% saline which was placed in the sonicator filled with approximately 47 °C tap water.

v) Xylene immersion time from 20 seconds to 20 minutes

Following xylene immersion, samples were either maintained in a sterile state by rinsing twice with 100% ethanol then storing the samples immersed in 100% ethanol in sealed petri dishes or they were allowed to dry overnight in a fume hood.

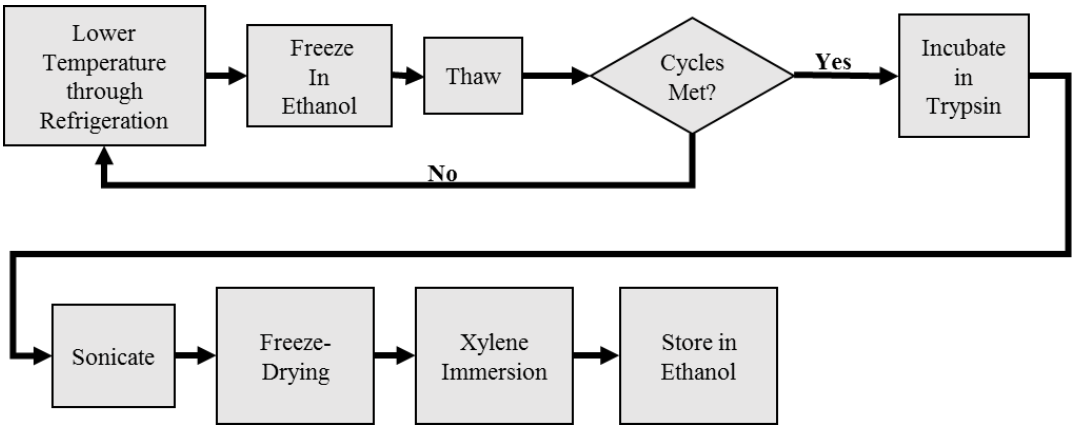

Figure 3.1: The finalized version of Method 2

Table 3.2: Conditions for sonication trials. *Typical indicates the preparation method was 4 freeze-thaw cycles, rinsing with PBS, 1.5hr incubation in trypsin-EDTA at 37°C, and rinsing with deionized water

Trial	Preparation Method	Time (min)	Solution	Solution Temp. (°C)	Comments
1	none	20	water	RT	control
2	none	60	water	RT	control
3	4 freeze-thaw cycles	60	trypsin-EDTA	RT	sample trypsinized for an additional 30 minutes at 37 °C
4	Typical*	60	water	RT	
5	Typical	60	water	46	pure hot tap water
6	Typical	30	water	50	
7	Typical	30	SDS	RT	sample was stored in 100% ethanol overnight before sonication
8	Typical	30	SDS	35	sample ~ 2 cm×3cm×3 mm
10	Typical	60	SDS	46	pure hot tap water, sample stored in 100% ethanol before sonication, sample ~1cm×2.5cm×3mm

3.3 DNA Content Analysis

3.3.1 DNA Extraction

200mg and 1000mg samples of fresh PAT were cut. The larger sample was decellularized and both samples were used in their entirety. The samples were ground in a mortar using a pestle and liquid nitrogen. 920µL of Biase's disruption solution [60] was added to the mortar and the samples were reground in liquid nitrogen to assist the disruption solution spread throughout the material. The samples were transferred to 2.0mL microcentrifuge tubes and an additional 920µL of disruption solution was added. The tubes were incubated at 60°C for 3 hours. 300µL of 6M NaCl was added, the samples were vortexed for 15 seconds, and they were centrifuged for 30 minutes at 14,100×g (Eppendorf MiniSpin plus, Eppendorf, Hamburg Germany). 500µL of each supernatant was collected and transferred to new tubes. 200µL of 25:24:1

phenol:chloroform:isoamyl alcohol was added to the tubes, they were vortexed for 15 seconds and centrifuged at 14,100×g for 10 minutes. Each supernatant was transferred to new microcentrifuge tubes and 500µL of cold isopropanol (1°C) was added. The combination was vortexed for 15 seconds and centrifuged at 14x100×g for 10 minutes. The liquid was decanted from the tubes leaving only the DNA pellet. 100% ethanol was added, the samples were centrifuged at 14,100×g for 10 minutes, the ethanol was pipetted out and the pellets were allowed to dry for 5-10 minutes. The pellets were suspended in 50µL of Tris-EDTA (TE) buffer, a buffer commonly used to solubilize DNA and improve its stability by inhibiting DNases, and incubated overnight at 1°C. They were then examined; un-dissolved pellets were forced into suspension by alternately heating the samples with hot tap water (~46°C) and vortexing them.

3.3.2 DNA Analysis

DNA concentration was measured directly using nanodrop spectrophotometry (Nanodrop 1000 Thermo Scientific, Waltham, MA). TE was used as the blank or background measurement to match the DNA suspension solution. Between each measurement, the pedestal was wiped using a laboratory wipe. 2µL of DI H_2O was pipetted onto the pedestal and it was wiped again. Each sample was measured four times. The average and standard deviation for the concentration of each measured sample was calculated. In addition, gel electrophoresis was used to validate DNA presence. The gel electrophoresis chamber (Enduro EPL-1007-7, Phenix Research Products, Candler, NC) had a pole to pole distance of approximately 18cm. Gels were 0.8% agarose in tris-acetate-EDTA (TAE) buffer. 7µL of sample or control, 2µL of loading buffer, and 1µL of ethidium bromide (500µg/ml) were loaded into two wells. TAE was used as the running buffer. The gels were run at 80V for 40 minutes. Imaging was performed using a UV gel imaging system (GelDoc-It with attached 6100 Series Gel HR Camera, UVP, Upland, CA, capture at either 308nm or 365nm) and the relative gel band intensities were found using ImageJ. The processed DNA mass fraction was calculated:

$$x_f\left[\frac{ng}{mg}\right] = W_p\left(\frac{0.5\text{ml Supernatant}}{1.84\text{ ml DS} + 0.3\text{ ml NaCl}}\right)\left(\frac{0.007\frac{\text{ml}}{\text{well}}}{0.05\text{ml TE Buffer}}\right)(7\mu\text{l})\ C_p$$

$$C_p\left[\frac{ng}{\mu L}\right] = \left(\frac{I_p}{I_u}\right)C_u\left[\frac{ng}{\mu L}\right]$$

x_f is the mass fraction in DNA per mg dry processed sample. W_p is the weight of the processed sample, DS is the disruption solution, C_p is the concentration of DNA extracted from the processed sample, $C_u$is the concentration of DNA extracted from the unprocessed sample. C_u was taken to be the upper error for the measured average unprocessed sample DNA concentration (average plus standard deviation).

3.4 HISTOLOGICAL MICROSCOPY

For optimization, histology slides were created after each step in the decellularization process. After processing (specific to each optimization step), samples were fixed in pure formalin (10% formaldehyde) overnight, rinsed with PBS 3 times, and stored in 100% ethanol until delivered to The Oklahoma Animal Disease and Diagnostics Laboratory (OADDL). OADDL embedded samples in paraffin from which 4 μm thick sections were cut. Sections were stained with hymatoxylin and eosin (H&E) and plated. Prepared slides were returned to the lab. Digital photomicrographs of various locations on each slide were captured by routine light microscopy using an inverted microscope with built-in color camera (AMG EVOS AME i2111, Life Technologies, Grand Island, NY).

3.5 SCANNING ELECTRON MICROSCOPY

A scanning electron microscope (SEM) (JEOL JSM-6360, JEOL USA Inc., Peabody, MA) was used to analyze the microstructure of processed PAT. The method used was similar to previous publication [61], with minor modifications. Samples were stored in a desiccator following after the xylene had evaporated from xylene immersed samples to maintain a low sample water content

until examination. During examination, samples were cut into squares approximately 0.5mm×0.5mm and embedded in carbon paint on the surface of an aluminum stub. Samples were sputter coated for 60 seconds. Digital micrographs were obtained at an 8kV accelerating voltage.

3.6 CELL SEEDING

IMR-32 (ATCC® CCL-127™) neuroblastoma were purchased from American Type Culture Collection *(*ATCC®*,* Manassas, VA, USA) and cultured with growth medium containing Eagle's Minimum Essential Medium (EMEM*)* following the vendor's protocol. In brief, neuroblastoma were maintained in EMEM containing 10% fetal bovine serum (FBS) on tissue culture plastic (TCP) at standard mammalian culture conditions (37°C, 5% CO_2, 95% air) in a humidified cell culture incubator. Growth medium was discarded and replaced every two days. When confluent, cells were harvested from the TCP using trypsin and neutralized with growth medium, centrifuged at 125×g for 5 minutes and resuspended in growth medium. D

Viable cells were counted using a Trypan blue dye exclusion assay. A 2 day cell seeding experiment was performed using 100,000 IMR-32 on samples approximately 1.5cm×1.5cm. In addition, an 8 day cell seeding experiment was performed, also with 100,000 IMR-32. The cells were pre-stained with a carboxyfluorescein diacetate-succinimidyl ester (CFDA-SE) green stain (Sigma Aldrich, St. Louis, MO) before seeding. CFDA-SE is inactive until it passively diffuses across the cellular membrane into the cytoplasm where its acetate groups are cleaved by esterases. After cleaving it becomes highly florescent and reacts with intracellular amines which prevent it from escaping the cell [62]. Cells in the scaffold were analyzed using both a Nikon Eclipse TE2000-U inverted microscope (using an attached CCD camera and Prior Scientific Lumen 200 florescence illumination system) and a Leica TCS SP2 Confocal System (Leica DM E14 with an argon ion laser, 488 nm excitation). A minimum of two processed PAT samples were seeded during each experiment.

A preliminary cell culture experiment was conducted using passage 5 human foreskin fibroblasts (HFF-1). The cell culture experiment was performed similarly to the neuroblastoma experiment. At day two, samples were fixed and processed for histology with H&E stain.

3.7 MECHANICAL CHARACTERIZATION

To characterize the mechanical properties of the scaffold, tensile samples were axially strained to break at a rate of 10mm/min. Afterwards, the viscoelasticity of the scaffold was examined via multi stage stress relaxation (MSSR). All testing was conducted at 37°C and the samples were submerged in PBS throughout the test period (hydrated conditions). Samples were cute to 1 cm wide by 2-4 cm in length using a polymer template.

Obtained sample widths were characterized from digital photographs of the sample under hydrated conditions with a rule next to it using ImageJ. Figure 3.2.a is an example photograph demonstrating the rule placed in-plane with the submerged sample and a picture taken perpendicularly to it to reduce errors. Multiple measures were made over the length of the sample and the average measure was taken as the sample width for all calculations.

To characterize sample thickness, digital micrographs were captured using an inverted microscope (Nikon Eclipse TE2000-U, Nikon, Tokyo, Japan) with attached CCD camera as previously described [33, 63]. Briefly, a sliver, approximately 0.5-1 mm in thickness, was cut from the edge of tissue. Samples were curled about themselves in a spiral and placed on a slide so that they were edge-on to it. Using image analysis software (Sigma Scan Pro, Systat Software, Point Richmond, CA, USA), multiple measurements were taken over multiple micrographs of each sample for both dry and DI H_2O wetted conditions (see Figure 3.2.b for an example micrograph). A same-magnification photomicrograph of a hemocytometer was used for the software's spatial calibration. The average thickness was calculated and used as the sample thickness in all calculations.

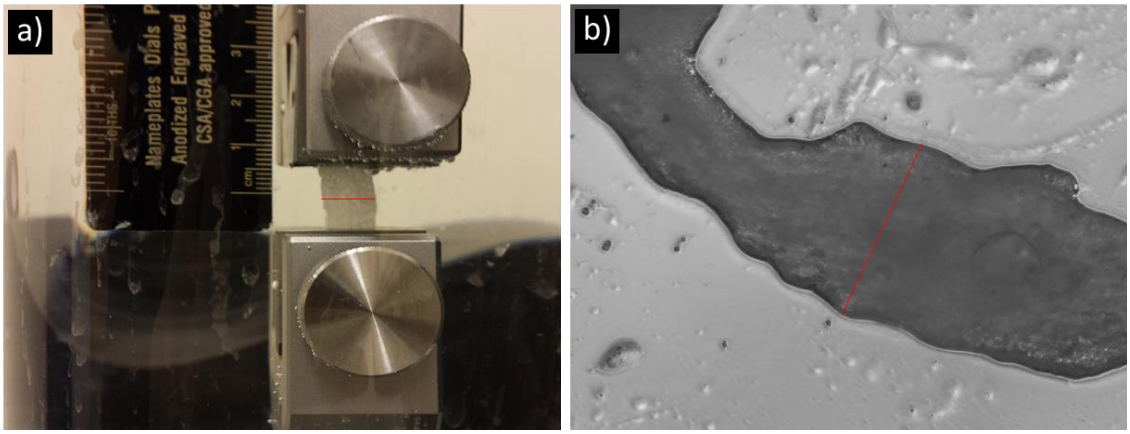

Figure 3.2: Width and thickness measurement examples. a) Example digital photograph used to determine the width of test sample and b) example photomicrograph used to find the thickness of a test sample (representative width lines shown in red).

3.7.1 Uniaxial Tensile Testing

Samples were strained to break at 10 mm/min crosshead speed using an INSTRON 5542 (INSTRON, Canton, MA, USA) to match testing conditions used for SIS [33]. The paired Merlin control and acquisition software was used to conduct tests and record data. Data was exported to Microsoft Excel. Break stress and strain were determined in Microsoft Excel using the average width and sample thickness (calculated as described above). The elastic modulus was calculated from the slope of the linear portion of the stress-strain curve.

3.7.2 MSSR

A set of four, 5-stage MSSR tests were conducted. The ultimate strain limit was determined from uniaxial tensile data and was chosen to prevent destruction of the sample. Samples were subjected to a constant step tensile strain applied at the rate of $3.125\%s^{-1}$ for 3.5s and 1.6s (10% and 5% strain per ramp respectively). Then the sample was allowed to relax for 60s. This was repeated up to either 50% or 25% strain. In addition, the reduced relaxation function,

G(t), was calculated by setting each stage's starting time to zero and normalizing each stage to the maximum stress experienced by the sample during that stage.

CHAPTER IV

RESULTS: OPTIMIZATION AND EVALUATION OF PAT

4.1 SMALL SAMPLE PREPARATION AND OPTIMIZATION

Initial sample preparation and optimization was conducted with samples approximately 1cm×1cm×1-2mm. The results below pertain to samples of this size. Scale up will be discussed later in this chapter.

4.1.1 Decellularization

We hypothesized that lipid removal would improve decellularization. Method 1 (section 3.1), which used methanol and chloroform was intended to remove lipids from the tissue. However, it destroyed the PAT sample and was discontinued.

Freeze-thawing damages cells. As water freezes, it crystalizes and the crystals pierce cell walls. Repeating this process by thawing and then refreezing the tissue causes additional damage. Because of its widespread use for decellularization [6, 26, 64-66], freeze-thawing was examined. Method 2 (section 3.2) shows the successful process incorporating this technique. A mixture of water and ethanol was used to increase water's miscibility in the lipids present in the native tissue. Hence, samples were submerged in an ethanol:water mixture before freezing. The ethanol percent was optimized by examining a range of ethanol mixtures (30%, 50%, and 70%, Figure 4.1 b-d and methods 1-3 in Appendix A). Histology slides were prepared to examine the effect. Using an ethanol concentration of 50% resulted in the fewest number of cell nuclei visible.

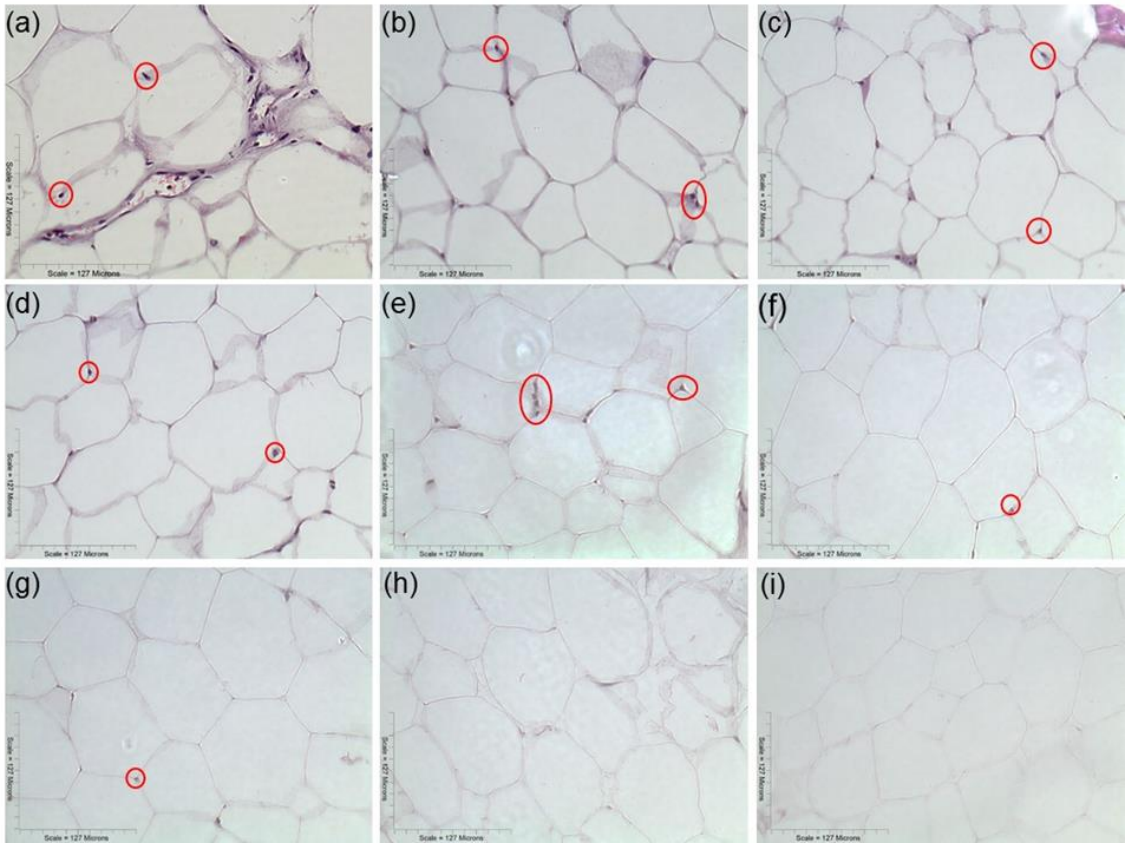

Figure 4.1: Micrographs of PAT after H/E staining at various processing steps: unprocessed PAT (a), the effects of varying the ethanol mixtures ((b) 30%, (c) 50%, and (d) 70%) with a single freeze-thaw cycle and 1 hr trypsination at 37°C, the effects of an increasing number freeze-thaw cycles ((e) 2, (f) 3, and (g) 4) with 50% ethanol and 1 hour of trypsination at 37°C, and finally, the effect of 4 freeze-thaw cycles using a 50% ethanol mixture and trypsin incubation times of 1.5 hr and 3 hr ((h) and (i) respectively). Representative cell nuclei are circled for clarity.

Therefore, 50% ethanol was chosen as the optimal concentration; the number of freeze-thaw cycles using this concentration was examined (1-4 cycles, methods 5-7 in Appendix A). Four freeze cycles resulted in the fewest visible cell nuclei. Trypsinization, routinely used in cell culture to suspend cells by cleaving attachment proteins, was used to cleave cells from the ECM. The incubation time was varied between 1.0, 1.5 and 3.0 hours (Figure 4.1 e-g, methods 8-10 in Appendix A) to obtain the maximum cell removal without damaging the ECM. Figure 4.1.h (method 9 in Appendix A) demonstrates the result of the optimization and satisfactory cell removal without damage to the ECM. Throughout this process, it was desirable to maintain short processing time. Therefore, given equal outcomes, the method requiring the shortest time period was chosen. Consequently, the optimization resulting in 4 freeze-thaw cycles in 50% ethanol with 1.5 hours of trypsinization, and was used for the rest of the study.

An initial cell seeding study conducted with HFF-1 resulted in a scaffold lacking cell nuclei. This result led to the initial assumption that preparing the sample in a biological safety cabinet (BSC) did not adequately protect the sample from contamination. Therefore samples were lyophilized for gas sterilization. The result, shown in Figure 4.2, demonstrates lipids drawn out of the tissue leading to the conclusion that, unexpectedly, decellularization occurred without significant lipid removal. No evidence of this unsuccessful lipid removal had been obtained earlier due to additional processing undergone by samples during histology. Moreover, it was assumed that decellularization was synonymous with successful lipid removal. This false assumption necessitated further processing. Based on the hypothesis that PAT maintained a hydrophobic environment and thereby prevented the cells, suspended in hydrophilic media, from infiltrating and attaching to the decellularized PAT. Therefore, a processes to remove lipids from the scaffold was created.

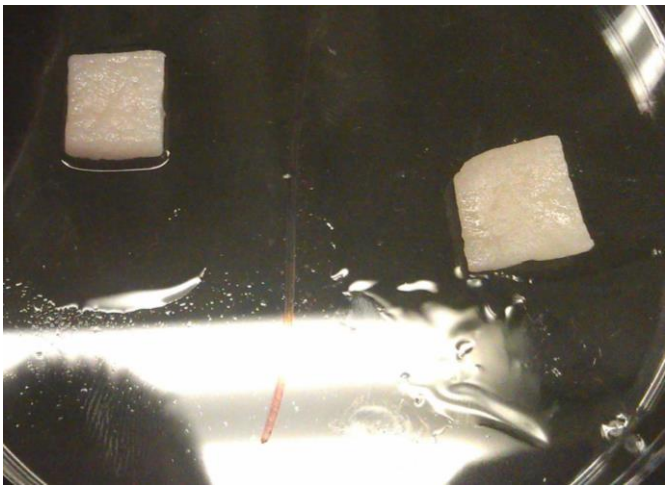

Figure 4.2: Lipid pool around lyophilized, processed scaffolds.

4.1.2 Lipid Removal

The effect of increasing concentrations of ethanol and increasing freeze-thaw cycles on the lipid content of the tissue was examined using lyophilization as the result. No effect was observed for up to 7 freeze-thaw cycles with a 90% ethanol solution. Therefore other means of lipid removal were sought.

Mechanical stimulation has often been used to extract cellular material from scaffolds [21, 22]. Hence, sonication was examined as a possible extraction method using several sonication solutions. Sonicating the scaffolds during the trypsinization step, with DI H_2O, and with SDS were examined. In addition, because of the low melting point of lipids, the effect of increasing the temperature of the sonication solution was examined. Sonicating PAT in SDS yielded visible results (Figure 4.3.a). Twenty minutes of sonication at room temperature resulted in a white scaffold (Figure 4.3.b).

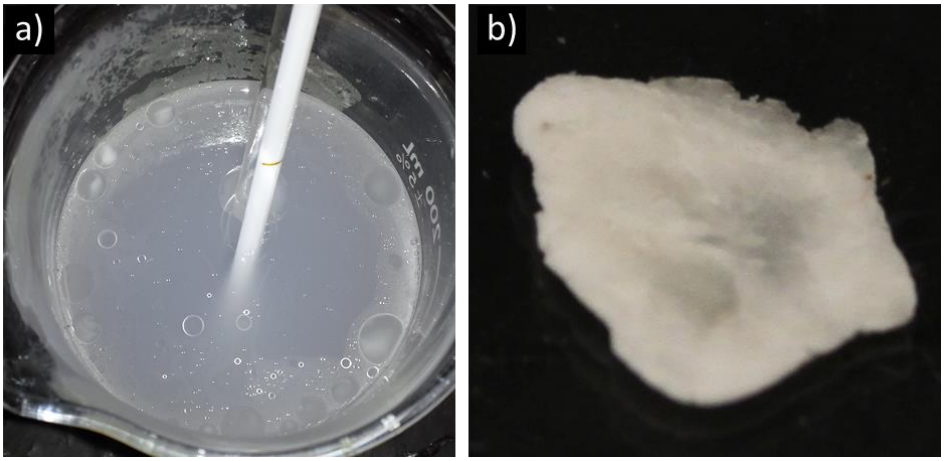

Figure 4.3: Visual sonication results. a) Lipids visible in SDS solution after sonication. b) White tissue obtained after 4 freeze-thaw cycles in 50% ethanol, 1.5 hours of trypsinization, and 20 minutes of sonication at 20°C.

4.2 Scale Up: Large Sample Preparation

Larger samples were desirable due to the difficulty of obtaining large numbers of small samples, the need for larger samples for mechanical testing, and to demonstrate successful scale-up to useful size. However, outcomes with larger samples cut by hand varied widely enough that it was impossible to ascertain the affect processing methods had on decellularization. To address this issue, a meat slicer was used to create uniform samples with a consistent thickness and to reduce diffusional variability between samples. This consistency allowed us to decellularize larger samples approximately 3cm×3cm×1mm. In addition to increasing uniformity, the food slicer cut thinner samples, improving the diffusional characteristics of the material. Samples with uniform thickness demonstrated a marked improvement in lipid removal and overall outcome.

When sonicating larger samples, heating the water in the sonicator led to greater lipid removal. Therefore, hot tap water (~47°C) was used as the sonication solution to increase bath temperature. To ensure the sample thawed completely before being refrozen a 1 hr thaw time at 37°C was adopted. However, samples were placed into the freezer directly after the thawing period.

Previously published articles indicate that the greater the temperature gradient experienced during freezing, the smaller the resulting crystals [16, 67]. This effect decreases the damage done to the cells during freezing and thawing. Therefore, the original thaw conditions (20 minutes at room temperature) were reinstated and a step to decrease the freezing temperature gradient was added: after samples thawed, they were placed in refrigeration (1°C) for 20 minutes before they were transferred to the freezer. Improved lipid removal was observed using this method, as determined by rubbing a processed sample between the thumb and forefinger and examining the oil expelled from the tissue. However, even with this additional step, lipids could be extracted from the tissue. Therefore, the ability of organic solvents to remove the remaining lipids from the scaffold was examined. Submerging samples in 0.208M acetic acid increased the oiliness of the scaffold surface after drying but failed to remove the lipids. Submerging samples in xylene for 20 seconds failed to remove sufficient lipids from the scaffolds. Increasing xylene submersion time to 17 minutes resulted in a lack of lipids being expunged from the tissue with mechanical stimulation. As a beneficial side effect, the use of xylene appears to sterilize the scaffolds (as evidenced by a successful 8-day cell culture following xylene immersion and storage in ethanol). Method 2, the final method, which successfully decellularized PAT and removed the lipids from it, is shown in Figure 3.1 (method 34 in Appendix A).

4.3 DNA REMOVAL

A primary requirement for using natural matrixes is ensuring removal of donor DNA components that could otherwise induce an inflammatory response and immune-mediated tissue rejection. To ensure processed PAT had a negligible amount of donor DNA, the DNA content of unprocessed and processed PAT was determined. First, nanodrop spectrophotometry was performed to directly measure DNA concentrations (Table 4.1). Following DNA extraction and suspension in TE buffer, the processed sample was milky. This observation was unsurprising since the processed sample weight was significantly greater than the weight of the unprocessed sample

and was comprised almost exclusively of ECM proteins. This observation also created a potential problem: nanodrop spectrophotometry results can be skewed by protein contamination. The a260/a280 ratio obtained for the processed sample supported the conclusion that the processed sample measurement was skewed by protein contamination. A secondary DNA quantification method was used to determine the concentration of the processed sample DNA.

Table 4.1: Nanodrop spectrophotometry results (n = 4, averages will be reported within this thesis as average±standard deviation; where n is the sample size).

Sample	**Concentration (ng/µL)**	**A260**	**260/280**	**260/230**
Unprocessed Sample	47.2±8.22	0.944±0.164	1.90±0.057	0.750±0.081
Processed Sample	31.3±2.19*	0.626±0.044	1.75±0.055	0.208±0.015

*Datum unreliable, refer to text for explanation.

DNA content in the processed sample was calculated by using unprocessed average DNA concentration plus one standard deviation as a worse case. ImageJ was used to find the intensity of each band and the relative band intensity of the processed sample, $\frac{I_p}{I_u}$, was calculated. In combination with the average measured weight reduction caused by processing (79.1±3.98%, n = 4) and the volumes and weights used for extraction, the DNA mass fraction of the unprocessed sample was calculated. Using the relative intensity, and unprocessed mass for each sample extracted, the DNA mass fraction was calculated. It was found to be 0.218 ng DNA per mg dry scaffold. The total reduction in DNA was also calculated; it was found to be 99.92%.

Crapo et al. [22] published an upper DNA mass fraction of 50 ng DNA per mg dry scaffold sufficient to prevent the sample from rejecting upon implantation. Compared to the 0.218 ng/mg mass fraction of the processed scaffold, this content is negligible compared to the published value. Therefore, Method 2 successfully decellularizes PAT.

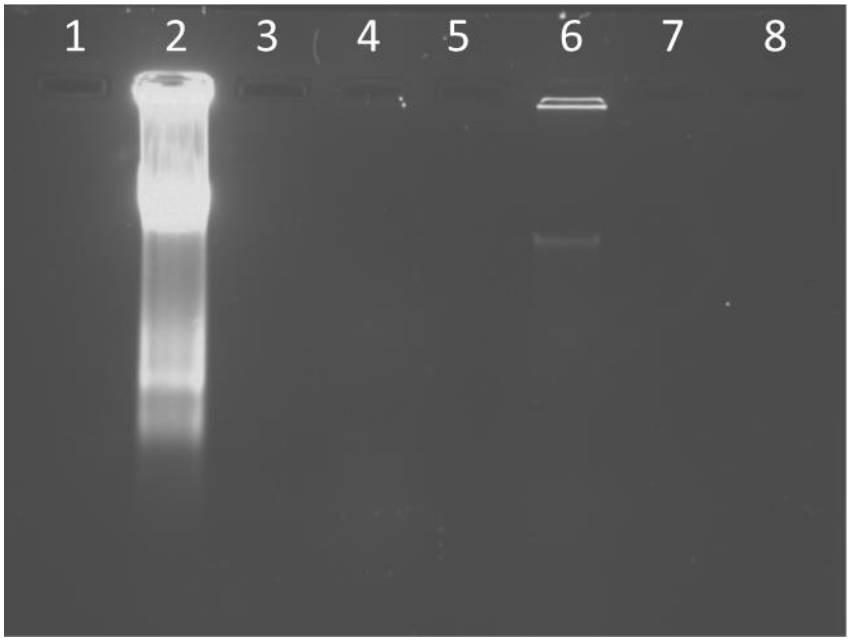

Figure 4.4: Image of 0.8% agarose gel run for 40 minutes at 80V. Lane 2 contains the unprocessed PAT sample. Lane 6 contains the processed PAT sample.

4.4 PROCESSED PAT MORPHOLOGY

Scaffold morphology, including pore size distribution, homogeneity, and channel structure are expected to strongly affect both cell ingrowth and nutrient distribution during the growth phase prior to angiogenesis. Naturally formed matrices have the desired architecture. To understand PAT's microarchitecture, samples were analyzed via SEM. SEM demonstrated that PAT lacks sidedness (Figure 4.5.a-b), unlike SIS. It further confirmed that PAT has a porous structure with a useful pore size (approximately 150 μm, Figure 4.5.c-d). Intact vascular structures were sought and an extensive vascular network was found (Figure 4.5.e). Moreover, It was confirmed that vascular tubes were present (Figure 4.5.f). As can be seen, cooling samples before freezing them does not appear to have changed the tissue microarchitecture appreciably (Figure 4.5.a,c,f were uncooled before freezing, Figure 4.5.b,d,e were cooled before freezing).

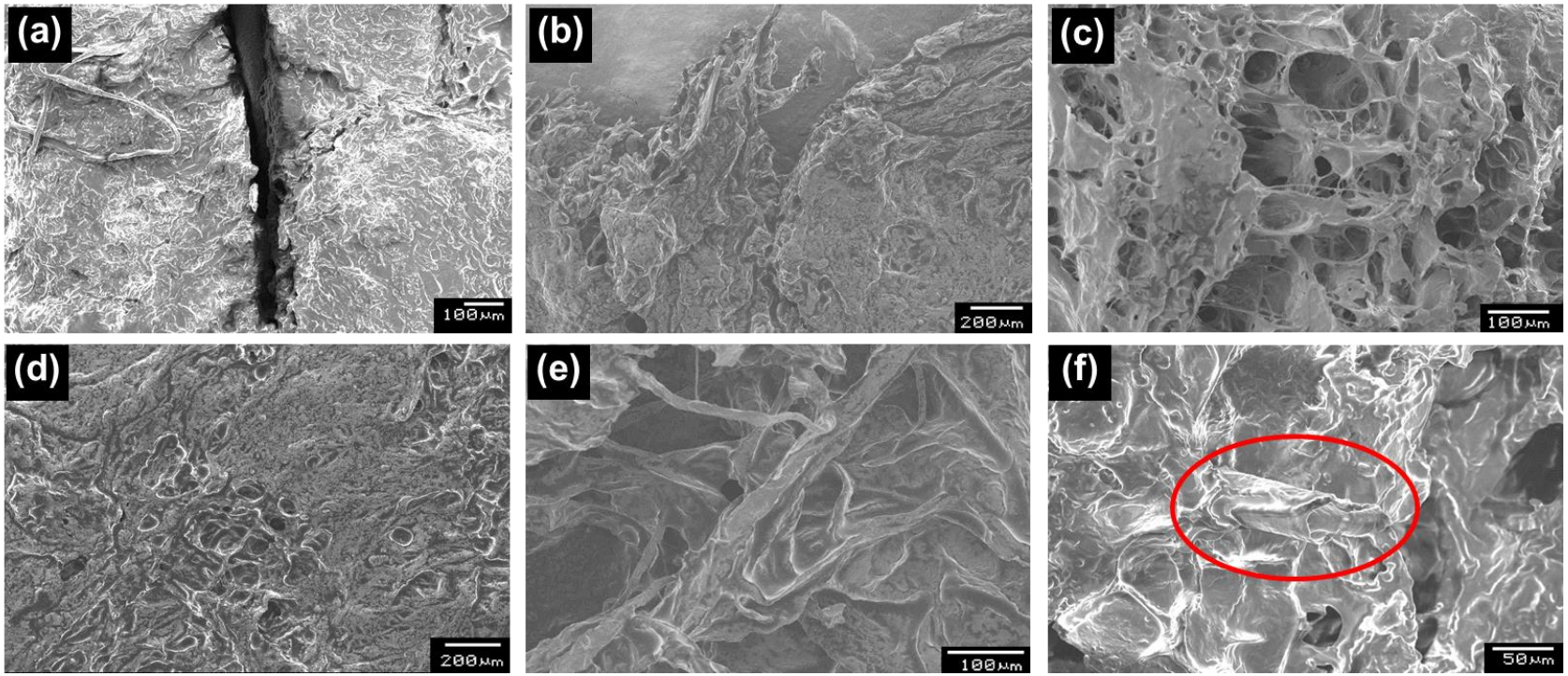

Figure 4.5: Microarchitecture of PAT after processing. Samples a, c and f did not have the temperature decrease step prior to freezing. Micrographs show (a-b) lack of sidedness, (c-d) porosity of processed sample, and (e-f) intact vascular structures.

To understand the thickness and variation of the samples cut with a meat slicer, several unprocessed samples were measured in multiple locations using a digital caliper. The average thickness was found to be 0.825±0.216mm (n = 5). Variation in sample thickness was attributed to both the gradual thawing of PAT during the cutting processes (initial cuts were frozen while the final few cuts were completely thawed), and to pressure and/or speed variation on the part of the user during cutting. Comparing this average thickness to SIS, it was almost four fold greater than SIS's 200μm thickness. In addition to measuring the initial thickness and determining the weight loss of the sample during processing (see section 4.3), the thickness change before and after processing was examined, as were the swelling properties of processed PAT (Table 4.2). The table demonstrates nearly 50% of the tissue thickness is lost during processing and PAT swells nearly 40% in DI H_2O. Combined with the weight lost during processing, this result strongly suggests the majority of lipids were removed from processed PAT since water was able to infiltrate the scaffold and it is known that lipids are the most abundant component of adipose tissue.

Table 4.2: Swelling properties of processed PAT.

Property	Sample 1	Sample 2	Sample 3	Average
Thickness—Dry (μm)	590±193	248±78.9	349±77.1	396±116
Thickness—Wet (μm)	734±128	462±28.1	492±56.6	563±70.9

4.5 CELL CULTURE

The importance of growth and attachment factors to cell ingrowth and viability was discussed earlier (section 2.1.3). Various steps in the decellularization process can affect these and other biological factors integral to the regenerative process. For example, trypsin cleaves peptide bonds and could damage both the ECM and its factors with prolonged exposure. Prolonged sonication can also damage the ECM. To determine whether cell attachment and cell ingrowth occurs, a 2 day and an 8 day cell seeding study were conducted in 6 well plates using IMR-32. At the end of the 2 day experiment, the tissue was fixed and processed. Figure 4.6.a demonstrates a

cells present at two days. However, the cells' round shape indicated a likely lack of attachment. However, the 8-day cell study, which used CFDA staining to allow cell imaging through the tissue without histological processing, demonstrated that cells proliferated evenly throughout the scaffold (Figure 4.6.b). Moreover, the non-spherical shape of the cells indicate cell attachment had occurred at this point. In addition, confocal microscopy was used to image cells through a range of the tissue thickness. A step size of 2.72μm was used and the constructed, full range image spans an 81.4μm thick portion of the scaffold. Cells were observed in every layer of the span giving evidence that cells successfully infiltrated the porous structure observed earlier through SEM. Again, cells were clearly not spherical and had attached to the scaffold. Finally, additional SEM work was conducted. Portions of the fixed scaffold from the 8 day experiment were dried overnight in a vacuum desiccator before they were cut, embedded in carbon paint on aluminum stubs, and sputter coated for 1 minute. Cells attached to the surface of the PAT were observed. In some locations, numerous lamellapodia and filapodia were observed to be anchored to the surface of the scaffold.

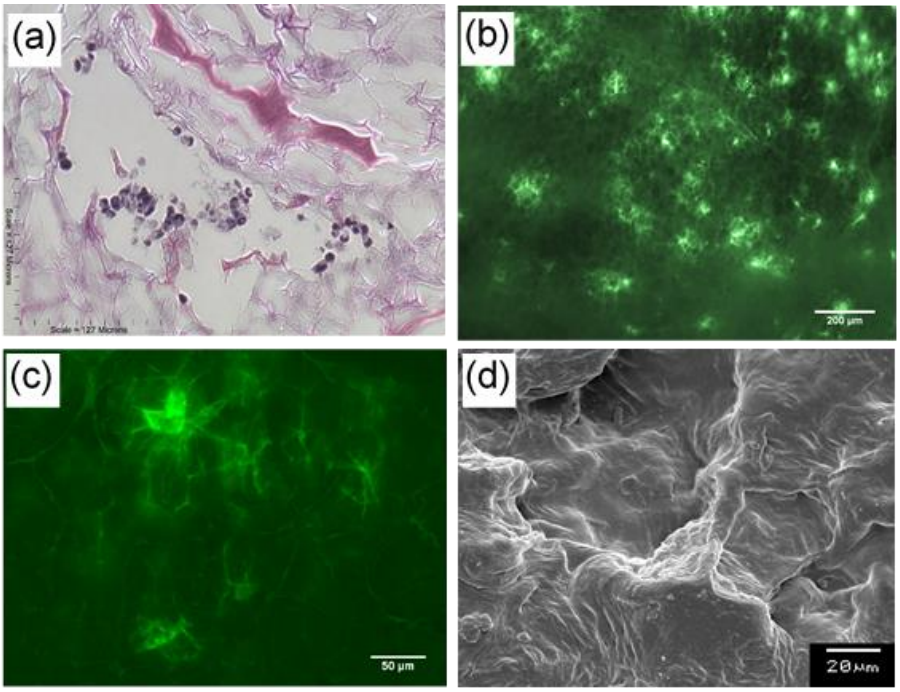

Figure 4.6: Cell culture results. a) H&E slide of tissue at the end of the 2-day cell seeding experiment. b) Florescent microscopy of the tissue at the end of 8 day cell seeding. c) Full range confocal, florescent microscopy results of 8 day seeded tissue. d) ECM image of cell attached along the ridge line shown near the center of the image.

4.6 TENSILE PROPERTIES

The uniaxial tensile properties of processed PAT were analyzed under hydrated conditions at 37°C. A representative sample's stress-strain curve is shown in Figure 4.7. Processed PAT demonstrated non-linear stress-strain behavior even at small strain ranges. The average ultimate tensile strength of multiple samples was 87.4±23.1kPa (n = 3) and the average break strain was 53.9±13.3% (n = 3). Variation beyond that normal for biological samples was attributed to perforations observed in the tissue. These perforations are likely vascular tubes (shown in Figure 4.5.e-f) cut perpendicular to their length during sample preparation. In addition to the presence of pores, even when special effort was made not to subject the scaffold to any more mechanical stress than absolutely necessary to complete processing these perforations still occurred in the material.

They were not visible to the naked eye and were therefore difficult to anticipate and cut around. Because of this difficulty, perforations are treated as a normal part of the tissue's mechanical characteristics and samples with these perforations were not excluded from the sample set.

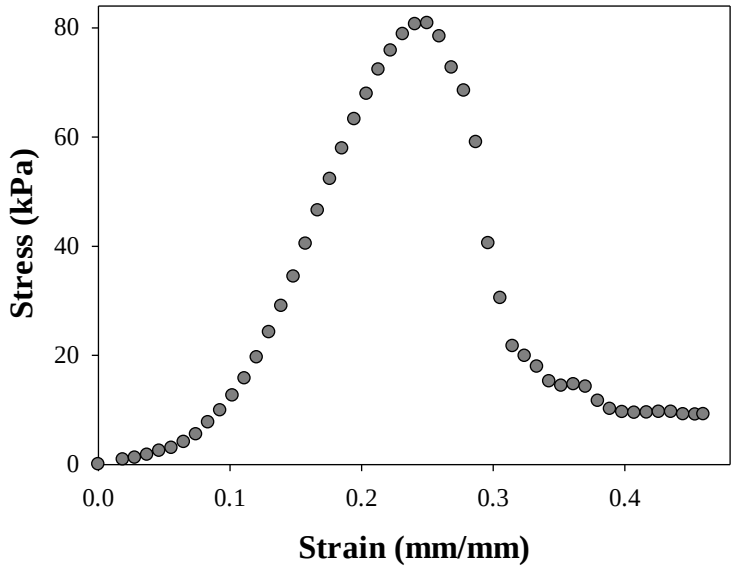

Figure 4.7: Representative stress-strain diagram for processed PAT. Uniaxial testing was conducted at 10 mm/min and 37°C in PBS.

Concerning the behavior of processed PAT, a typical tissue J-curve is observed, as discussed in the background in section 2.3.1. Clearly, non-linear behavior is observed throughout the loading portion of the diagram and it is difficult to isolate a single linear region with which to evaluate an elastic modulus. Despite this, a semi-linear region was observed between 14% and 20% strain. This region was used to calculate the elastic modulus of the sample with a least squares regression for each sample. The average elastic modulus was 324±141 kPa (n = 3). However, as Figure 4.7 demonstrates, the entire curve is non-linear. Therefore the elastic modulus is a highly variable value and should not be relied upon. Due to the non-linearity of processed PAT, stress-relaxation testing was performed. Comparing processed PAT to SIS, PAT has a much lower

ultimate tensile stress and elastic modulus (87.4kPa vs. 22.6-61.3MPa and 324kPa vs. 8.28-42.0MPa for the ultimate tensile stress and elastic moduli respectively).

4.7 MSSR

To explore the viscoelastic properties of processed PAT multiple 5-stage multi-stage stress-relaxation experiments were conducted congruent to previous testing methods. Reported results from similar experiments for SIS used a 15% loading per ramp and 100 seconds of relaxation over 4 ramps in hydrated conditions [46]. For PAT, the total sample strain was reduced to 30%, to ensure the sample remained intact. SIS and other soft tissues demonstrate strain hardening behavior [68]; this same behavior was observed for PAT after processing (Figure 4.8.a). As processed PAT was stretched in the first stage, the stress developed was significantly less than that developed in the fifth stage. The relaxation behavior was different from that of chitosan and chitosan/gelatin porous scaffolds [25], polycaprolactone (PCL) scaffolds [26] and 50:50 poly-lactide-co-glycolide (PLGA) films [27]. Chitosan and chitosan-gelatin scaffolds showed no change in stress accumulation in successive stages. The stress accumulation of PLGA films decreased in successive stages, leading to strain softening. This difference could be attributed to the fact that 50:50 PLGA is an amorphous polymer whereas PCL is a semi-crystalline polymer.

To better examine variation in profile between the stages, each stage was normalized by taking the ratio $\frac{\sigma(t)}{\sigma_{max}}$ where $\sigma(t)$ is the stress at any given point in a stage with the beginning of each ramp to $t = 0$, defined as the beginning of the stage and σ_{max} is the maximum stress developed in that stage which occurred at the end of the linear ramp. This is called the reduced relaxation function G(t) and is described by Fung [39]. Figure 4.8.b shows the reduced relaxation function for each stage plotted simultaneously. Both SIS and PAT experience an initial conditioning period. As can be seem, the first stage profile is significantly different than the 2-5 stages and significantly greater relaxation is observed during the first stage. This is expected for

tissues [39]. As can be seen, PAT shows a nearly 30% relaxation from the maximum stress in each stage. This can be compared with chitosan scaffolds which show 90% relaxation at the end of each stage and with PCL which show 25% relaxation at the end of each stage.

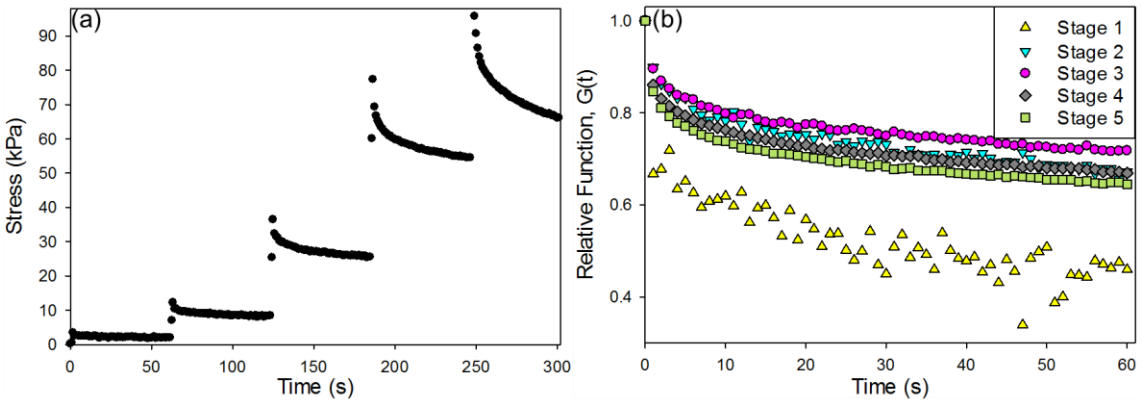

Figure 4.8: Results of a characteristic MSSR experiment. a) MSSR stress vs time curve. b) The reduced, relative function vs time.

CHAPTER V

CONCLUSIONS AND RECOMMENDATIONS: PRESENT TO FUTURE

5.1 CONCLUSIONS

This study examined multiple non-toxic decellularization steps and a single toxic lipid removal step applicable to the native soft tissues. Optimization of the decellularization methods was performed to meet the specific aims stated at the beginning of this thesis. Moreover, the properties of the scaffold were determined, demonstrating the success of the developed process and comparing the developed scaffold to other soft tissue scaffolds; both those clinically available and those under investigation, with an emphasis on SIS as the most successful soft tissue scaffold currently available. The findings of this study will be stated within the framework of the specific aims presented at the beginning of this work:

1. *Create a process that decellularizes PAT while maintaining its natural morphology.*
    - The final process developed to decellularize PAT was shown in Figure 3.1. Freeze-thawing caused minimal damage to the ECM and could be used in conjunction with trypsinization to successfully decellularize PAT and was therefore optimized. Additional steps were required to remove the lipid content of PAT and therefore additional sonication, lyophilization, and xylene immersion steps were introduced to remove the lipids from the unprocessed tissue.

- Cell seeding experiments demonstrated cellular attachment to the processed scaffold. In addition, the experiments demonstrate cells spread throughout the matrix and are viable after 8-days.
- The DNA content of processed PAT was examined and near total removal of DNA (99.92%) was demonstrated. Moreover, by examining the absolute mass fraction of DNA in the processed scaffold on a dry basis, it was determined that processed PAT contains 0.218 DNA per mg dry scaffold. Comparing this value to literature it was found to be negligible compared to the decellularization level that is likely to cause immune rejection.

2. *Characterize PAT's mechanical and physical properties.*

To characterize processed PAT, its morphology and microarchitecture were examined, multiple mechanical properties of the processed scaffold were determined and compared to clinically available scaffolds and to scaffolds under investigation in the literature.

- As stated in the objective, a scaffold that maintained PAT's native tissue morphology was sought. Through visual microscopy of PAT throughout the decellularization steps, it was demonstrated that PAT's native morphology remained intact. In addition, the microarchitecture was examined using SEM. Through SEM micrographs, it was demonstrated that processed PAT is porous, that a network of vascular channels does remain intact within the tissue in an un-collapsed state, and that the microscale morphology of PAT is mainly homogeneous without distinct regions that differ strongly from others in segregated areas. This includes a lack of sidedness, a major heterogeneity seen in SIS.
- Tensile testing conducted on processed PAT led to quantification of the average break stress and strain of the processed scaffold: 87.4±23.1 kPa and 53.9±13.3%

respectively. Moreover, an approximate elastic modulus of 324±141 kPa was found between 14% and 20% strain.

- 5-stage MSSR testing was conducted and demonstrated that PAT has an initial conditioning period followed by consistent percent relaxation and strain hardening behavior (increasing stress per ramp). In addition the relaxation behavior was compared to SIS, and found both to be strain hardening and found both to have the initial conditioning period. The stress-relaxation properties were also compared to chitosan, chitosan-gelatin, polycaprolactone, and PLGA films.

5.2 OUTLOOK

The ultimate goal for any practical technology is commercialization. PAT requires significant work before it will be ready for commercialization. The first step along that path will be to utilize an *in vivo* animal model to explore the immunogenicity of the tissue. Second, although many growth factors are known to be present in adipose tissues, the growth factors remaining in PAT after processing have yet to be determined. Further experiments are necessary to quantify these properties. In addition, to further quantify the viscoelastic properties of PAT, dynamic mechanical analysis, a form of cyclical testing will provide additional insight.

REFERENCES

[1] Badylak SF, Weiss DJ, Caplan A, Macchiarini P. Engineered whole organs and complex tissues. The Lancet. 2012;379:943-52.

[2] Jana S, Tefft BJ, Spoon DB, Simari RD. Scaffolds for tissue engineering of cardiac valves. Acta Biomaterialia. 2014;10:2877-93.

[3] Organ Procurement and Transplantation network, Scientific Registry of Transplant Recipients. OPTN/SRTR 2012 Annual Data Report. In: Department of Health and Human Services, Health Resources and Services Administration, editors. Rockville, MD 2014.

[4] Wang L, Johnson JA, Chang DW, Zhang Q. Decellularized musculofascial extracellular matrix for tissue engineering. Biomaterials. 2013;34:2641-54.

[5] Poon CJ, Pereira E. Cotta MV, Sinha S, Palmer JA, Woods AA, Morrison WA, et al. Preparation of an adipogenic hydrogel from subcutaneous adipose tissue. Acta Biomaterialia. 2013;9:5609-20.

[6] Georgiou M, Bunting SCJ, Davies HA, Loughlin AJ, Golding JP, Phillips JB. Engineered neural tissue for peripheral nerve repair. Biomaterials. 2013;34:7335-43.

[7] Badylak SF. The extracellular matrix as a biologic scaffold material. Biomaterials. 2007;28:3587-93.

[8] Vyavahare N, Ogle M, Schoen FJ, Zand R, Gloeckner DC, Sacks M, et al. Mechanisms of bioprosthetic heart valve failure: fatigue causes collagen denaturation and glycosaminoglycan loss. J Biomed Mater Res. 1999;46:44-50.

[9] Service. UNAS. United States Department of Agriculture: National Agricultural Statistics Service. USDA; 2014.

[10] Ingber DE. Mechanical signaling and the cellular response to extracellular matrix in angiogenesis and cardiovascular physiology. Circulation research. 2002;91:877-87.

[11] Engler AJ, Sen S, Sweeney HL, Discher DE. Matrix Elasticity Directs Stem Cell Lineage Specification. Cell. 2006;126:677-89.

[12] Hong JK, Madihally SV. Next Generation of Electrosprayed Fibers for Tissue Regeneration. Tissue Eng Part B-Re. 2011;17:125-42.

[13] Braghirolli DI, Steffens D, Pranke P. Electrospinning for regenerative medicine: a review of the main topics. Drug Discov Today. 2014;19:743-53.

[14] Billiet T, Vandenhaute M, Schelfhout J, Van Vlierberghe S, Dubruel P. A review of trends and limitations in hydrogel-rapid prototyping for tissue engineering. Biomaterials. 2012;33:6020-41.

[15] Tang ZY, Wang Y, Podsiadlo P, Kotov NA. Biomedical applications of layer-by-layer assembly: From biomimetics to tissue engineering. Adv Mater. 2006;18:3203-24.

[16] Virtual prototyping & bio manufacturing in medical applications: Springer Science+Business Media, LLC; 2008.

[17] Podichetty JT, Madihally SV. Modeling of porous scaffold deformation induced by medium perfusion. J Biomed Mater Res Part B. 2014;102:737-48.

[18] Ratakonda S, Sridhar UM, Rhinehart RR, Madihally SV. Assessing viscoelastic properties of chitosan scaffolds and validation with cyclical tests. Acta Biomaterialia. 2012;8:1566-75.

[19] Huang Y, Onyeri S, Siewe M, Moshfeghian A, Madihally SV. In vitro characterization of chitosan-gelatin scaffolds for tissue engineering. Biomaterials. 2005;26:7616-27.

[20] Sullivan DC, Mirmalek-Sani S-H, Deegan DB, Baptista PM, Aboushwareb T, Atala A, et al. Decellularization methods of porcine kidneys for whole organ engineering using a high-throughput system. Biomaterials. 2012;33:7756-64.

[21] Gilbert TW, Sellaro TL, Badylak SF. Decellularization of tissues and organs. Biomaterials. 2006;27:3675-83.

[22] Crapo PM, Gilbert TW, Badylak SF. An overview of tissue and whole organ decellularization processes. Biomaterials. 2011;32:3233-43.

[23] Sano H, Orbay H, Terashi H, Hyakusoku H, Ogawa R. Acellular adipose matrix as a natural scaffold for tissue engineering. Journal of Plastic, Reconstructive & Aesthetic Surgery. 2014;67:99-106.

[24] Dunne LW, Huang Z, Meng W, Fan X, Zhang N, Zhang Q, et al. Human decellularized adipose tissue scaffold as a model for breast cancer cell growth and drug treatments. Biomaterials. 2014;35:4940-9.

[25] Yu C, Bianco J, Brown C, Fuetterer L, Watkins JF, Samani A, et al. Porous decellularized adipose tissue foams for soft tissue regeneration. Biomaterials. 2013;34:3290-302.

[26] Flynn LE. The use of decellularized adipose tissue to provide an inductive microenvironment for the adipogenic differentiation of human adipose-derived stem cells. Biomaterials. 2010;31:4715-24.

[27] Brown BN, Freund JM, Han L, Rubin JP, Reing JE, Jeffries EM, et al. Comparison of Three Methods for the Derivation of a Biologic Scaffold Composed of Adipose Tissue Extracellular Matrix. Tissue Eng Part C-Methods. 2011;17:411-21.

[28] Choi JS, Kim BS, Kim JY, Kim JD, Choi YC, Yang H-J, et al. Decellularized extracellular matrix derived from human adipose tissue as a potential scaffold for allograft tissue engineering. Journal of Biomedical Materials Research Part A. 2011;97A:292-9.

[29] Sachlos E, Czernuszka J. Making tissue engineering scaffolds work. Review: the application of solid freeform fabrication technology to the production of tissue engineering scaffolds. Eur Cell Mater. 2003;5:39-40.

[30] Ignotz RA, Heino J, Massague J. Regulation of cell adhesion receptors by transforming growth factor-beta. Regulation of vitronectin receptor and LFA-1. J Biol Chem. 1989;264:389-92.

[31] Ignotz RA, Massague J. Cell adhesion protein receptors as targets for transforming growth factor-beta action. Cell. 1987;51:189-97.

[32] Badylak SF. The extracellular matrix as a biologic scaffold material. Biomaterials. 2007;28:3587-93.

[33] Raghavan D, Kropp BP, Lin HK, Zhang Y, Cowan R, Madihally SV. Physical characteristics of small intestinal submucosa scaffolds are location-dependent. Journal of Biomedical Materials Research Part A. 2005;73:90-6.

[34] Wood JD, Enser M, Whittington FM, Moncrieff CB, Kempster AJ. Backfat composition in pigs: Differences between fat thickness groups and sexes. Livestock Production Science. 1989;22:351-62.

[35] Zheng MH, Chen J, Kirilak Y, Willers C, Xu J, Wood D. Porcine small intestine submucosa (SIS) is not an acellular collagenous matrix and contains porcine DNA: Possible implications in human implantation. J Biomed Mater Res Part B. 2005;73B:61-7.

[36] Revi D, Vineetha VP, Muhamed J, Rajan A, Anilkumar TV. Porcine cholecyst–derived scaffold promotes full-thickness wound healing in rabbit. Journal of tissue engineering. 2013;4:2041731413518060.

[37] Thermo Scientific. T042-TECHNICAL BULLETIN NanoDrop Spectrophotometers: Assessment of Nucleic Acid Purity. Wilmington, DE: Thermo Scientific Nanodrop Products.

[38] Şenel Ayaz HG, Perets A, Ayaz H, Gilroy KD, Govindaraj M, Brookstein D, et al. Textile-templated electrospun anisotropic scaffolds for regenerative cardiac tissue engineering. Biomaterials. 2014;35:8540-52.

[39] Fung YC. Biomechanics: Mechanical Properties of Living Tissues: Springer New York; 1993.

[40] Holzapfel GA. Biomechanics of soft tissue. Boston: Academic Press; 2001.

[41] Sethuraman V. Viscoelastic modeling of stress relaxation behavior in biodegradable polymers: Oklahoma State University; 2013.

[42] Alkhouli N, Mansfield J, Green E, Bell J, Knight B, Liversedge N, et al. The mechanical properties of human adipose tissues and their relationships to the structure and composition of the extracellular matrix. Am J Physiol-Endocrinol Metab. 2013;305:E1427-E35.

[43] Fung Y. Elasticity of soft tissues in simple elongation. Am J Physiol. 1967;213:1532-44.

[44] Hatami-Marbini H. Hydration Dependent Viscoelastic Tensile Behavior of Cornea. Ann Biomed Eng. 2014;42:1740-8.

[45] Gautieri A, Vesentini S, Redaelli A, Ballarini R. Modeling and measuring visco-elastic properties: From collagen molecules to collagen fibrils. Int J Non-Linear Mech. 2013;56:25-33.

[46] Mirani RD, Pratt J, Iyer P, Madihally SV. The stress relaxation characteristics of composite matrices etched to produce nanoscale surface features. Biomaterials. 2009;30:703-10.

[47] Duling RR, Dupaix RB, Katsube N, Lannutti J. Mechanical Characterization of Electrospun Polycaprolactone (PCL): A Potential Scaffold for Tissue Engineering. Journal of Biomechanical Engineering. 2008;130:011006-.

[48] Shazly TM, Artzi N, Boehning F, Edelman ER. Viscoelastic adhesive mechanics of aldehyde-mediated soft tissue sealants. Biomaterials. 2008;29:4584-91.

[49] Peña E, Peña JA, Doblaré M. On modelling nonlinear viscoelastic effects in ligaments. Journal of Biomechanics. 2008;41:2659-66.

[50] Wang JL, Parnianpour M, Shirazi-Adl A, Engin AE, Li S, Patwardhan A. Development and validation of a viscoelastic finite element model of an L2/L3 motion segment. Theoretical and Applied Fracture Mechanics. 1997;28:81-93.

[51] Kohandel M, Sivaloganathan S, Tenti G. Estimation of the quasi-linear viscoelastic parameters using a genetic algorithm. Mathematical and Computer Modelling. 2008;47:266-70.

[52] Kochhar A, Wu I, Mohan R, et al. A comparison of the rheologic properties of an adipose-derived extracellular matrix biomaterial, lipoaspirate, calcium hydroxylapatite, and cross-linked hyaluronic acid. JAMA Facial Plastic Surgery. 2014.

[53] Ghosh P, Rameshbabu AP, Dhara S. Citrate Cross-Linked Gels with Strain Reversibility and Viscoelastic Behavior Accelerate Healing of Osteochondral Defects in a Rabbit Model. Langmuir. 2014;30:8442-51.

[54] Mintz BR, Cooper JA, Jr. Hybrid hyaluronic acid hydrogel/poly(ε-caprolactone) scaffold provides mechanically favorable platform for cartilage tissue engineering studies. Journal of biomedical materials research Part A. 2014;102:2918-26.

[55] Ghezzi CE, Marelli B, Donelli I, Alessandrino A, Freddi G, Nazhat SN. The role of physiological mechanical cues on mesenchymal stem cell differentiation in an airway tract-like dense collagen–silk fibroin construct. Biomaterials. 2014;35:6236-47.

[56] Dejardin LM, Arnoczky SP, Ewers BJ, Haut RC, Clarke RB. Tissue-engineered rotator cuff tendon using porcine small intestine submucosa Histologic and mechanical evaluation in dogs. The American journal of sports medicine. 2001;29:175-84.

[57] Dunphy SE, Bratt JAJ, Akram KM, Forsyth NR, El Haj AJ. Hydrogels for lung tissue engineering: Biomechanical properties of thin collagen–elastin constructs. Journal of the Mechanical Behavior of Biomedical Materials. 2014;38:251-9.

[58] Suki B. Assessing the Functional Mechanical Properties of Bioengineered Organs With Emphasis on the Lung. Journal of Cellular Physiology. 2014;229:1134-40.

[59] Budynas RG, Nisbett JK, Shigley JE. Shigley's mechanical engineering design: McGraw-Hill; 2008.

[60] Biase FH, Franco MM, Goulart LR, Antunes RC. Protocol for extraction of genomic DNA from swine solid tissues. Genetics and Molecular Biology. 2002;25:313-5.

[61] Hong JK, Madihally SV. Three-dimensional scaffold of electrosprayed fibers with large pore size for tissue regeneration. Acta Biomaterialia. 2010;6:4734-42.

[62] Molecular Probes. Vybrant® CFDA SE Cell Tracer Kit. Molecular Probes. Eugene, OR: Invitrogen; 2006.

[63] Lawrence BJ, Maase EL, Lin HK, Madihally SV. Multilayer composite scaffolds with mechanical properties similar to small intestinal submucosa. Journal of Biomedical Materials Research Part A. 2009;88:634-43.

[64] Badylak SF, Freytes DO, Gilbert TW. Extracellular matrix as a biological scaffold material: Structure and function. Acta Biomater. 2009;5:1-13.

[65] Benders KEM, Weeren PRv, Badylak SF, Saris DBF, Dhert WJA, Malda J. Extracellular matrix scaffolds for cartilage and bone regeneration. Trends in Biotechnology. 2013;31:169-76.

[66] Luo JC, Chen W, Chen XH, Qin TW, Huang YC, Xie HQ, et al. A multi-step method for preparation of porcine small intestinal submucosa (SIS). Biomaterials. 2011;32:706-13.

[67] Madihally SV, Matthew HWT. Porous chitosan scaffolds for tissue engineering. Biomaterials. 1999;20:1133-42.

[68] Rubin MB, Bodner SR, Binur NS. An elastic-viscoplastic model for excised facial tissues. J Biomech Eng. 1998;120:686-9.

APPENDIX A

Full list of optimization steps for Method 2 (continued onto next page):

Method	Freeze Solution	Freeze Temp (°C)	Number of Freeze-Thaw Cycles	Thaw Time (min)	Trypsination time at 37°C (hr)	Approximate Sample Size	Testing Method	Additional Treatment	Notes and Results
Cellular Removal Optimization									
1	30% EtOH	-81	1	20	1.0	~ 1x1x.2 cm	Histology H&E Stain		fewer nuclei observed in 50% EtOH Solution
2	50% EtOH								
3	70% EtOH								
4	50% EtOH	-81	1	20	1.0	~ 1x1x.2 cm	Histology H&E Stain		Examination under scope indicated 4 freeze-thaw cycles optimal
5			2						
6			3						
7			4						
8	**50% EtOH**	**-81**	**4**	**20**	1.0	**~ 1x1x.2 cm**	Histology H&E Stain		Examination under scope indicated 1.5 hr of trypsination sufficient to remove cell nuclei
9					**1.5**				
10					3.5				
11	50% EtOH	-81	4		1.5	~ 1x1x.2 cm	Cell Seeding		histology of seeded tissue did not show nuclei
12	50% EtOH	-81	4	20	3.0	R = 10 cm, .5 cm			freeze drying showed oily film, lipid content not removed (did not seed samples)
Lipid Removal Optimization									
13	none	-81	1	20	1.0	~ 1x1x.2 cm	Homogenization		no fat content reduction
14	100% EtOH								no fat content reduction
15	50% EtOH								no fat content reduction
16	70% EtOH								no fat content reduction
17	Deionized H_20								no fat content reduction
18a	75% EtOH	-81	4	20	1.5	~ 2 mm	Freeze-drying		Also soaked in ethanol before freezing to allow for diffusion. Still had oily substance upon freeze drying.
18b	90% EtOH					~ 0.5 mm			
18c	75% EtOH					~ 2 mm			
18d	90% EtOH					~ 0.5 mm			
19a	50% EtOH	-81	6	60	1.5	~ 1x1x.2 cm	Freeze-drying	• 24 hr in 100% EtOH	All samples had oily lipid film on petri dish. Addititonal lipid content could be rubbed from samples.
19b			6		1.5				
19c			6		3			• 24 hr in 100% EtOH	
19d			6		3				
20a			7		1.5			• 24 hr in 100% EtOH	
20b			7		1.5				
20c			7		3			• 24 hr in 100% EtOH	
20d			7		3				

21	none	N/A	none	N/A	none	~ 1x1x.2 cm	Freeze-drying	20 min in sonicator	lipid still present
22								• 1 hr in trypsin in sonicator at room temp	lipid still present
23								• 1 hr sonication in water separate from trypsination	lipid still present
24	50% EtOH	-81	4	60	1.5	~ 1x1x.2 cm	Freeze-drying	• 1 hr sonication in water at 46°C	lipid still present
25								• 1 hr sonication in water at 50°C	lipid still present
26								**• 1 hr sonication in SDS at Room Temp**	**lipid mostly removed**
Lipid Removal: Larger Samples									
27						~4x4x.1 cm		• frozen from 1°C	lipid mostly removed
28						~4x4x.2 cm		• 20 min sonication	lipid still present
29	50% EtOH	-81	4	60	1.5	~4x4x.1 cm	Freeze-drying	• 20 min sonication	lipid mostly removed, 27 appeared superior
30						~4x4x.2 cm			lipid still present
31						~4x4x.1 cm		• 20 min sonication • immersed in .21 M acetic acid for 30 minutes	lipid mostly removed
32						~4x4x.1 cm	Visual Examination and Mechanical Massaging	• 20 min sonication • immersed in histological grade xylene for 20 seconds	lipid mostly removed
33	50% EtOH	-81	4	60	1.5	~4x4x.1 cm		• 20 min sonication • immersed in hystological grade xylene for 17 minutes	Lipid completely removed
34						**~4x4x.1 cm**		**• 20 min sonication • immersed in hystological grade xylene for 20 minutes**	**Lipid completely removed, no improvement over 33**

VITA

Kevin D Roehm

Candidate for the Degree of

Master of Science

Thesis: DEVELOPING A SCAFFOLD FROM PORCINE ADIPOSE TISSUE

Major Field: Chemical Engineering

Biographical:

Education:

Completed the requirements for the Master of Science in Chemical Engineering at Oklahoma State University, Stillwater, Oklahoma in December, 2014.

Completed the requirements for the Bachelor of Science in Biosystems Engineering with a Biomechanical Option Oklahoma State University, Stillwater, Oklahoma in May, 2013.

Experience:

Oklahoma State University Graduate Teaching Assistant: Taught one or multiple discussion sections, held office hours, graded homework, graded and proctored exams. Classes were Fluid Mechanics, ENSC 3233, and Thermodynamics, ENSC 2213 from August 2013 to December 2014

Engineering Intern: Worked for Orthocare Innovations LLC. between May and August 2013. Worked on the design for a hydraulic pressurization and cycling system used to fill a closed loop hydraulic system in a prosthesis a flexible rubber cover for the prosthesis, and modifying and updating a cyclical test rig.

Wentz Research Scholar: Worked as an undergraduate researcher in Dr. Madihally's lab from 2012-2013.

Professional Memberships:

Alpha Epsilon—Biosystems and Agricultural Engineering Honor Society

Tissue Engineering and Regenerative Medicine International Society Member